Modern dextral strain controls active hydrothermal systems in the southeastern Canadian Cordillera

Article *in* Geological Society of America Bulletin · November 2022

DOI: 10.1130/B36500.1

5 authors, including:

Theron Finley
University of Victoria
21 PUBLICATIONS **34** CITATIONS
SEE PROFILE

Stephen T. Johnston
University of Alberta
201 PUBLICATIONS **5,220** CITATIONS
SEE PROFILE

Martyn Jonathan Unsworth
University of Alberta
235 PUBLICATIONS **9,050** CITATIONS
SEE PROFILE

Dinu Pana
Alberta Energy Regulator & University of Alberta
60 PUBLICATIONS **1,179** CITATIONS
SEE PROFILE

Statement

A previous version of this manuscript was submitted to GSA Bulletin on March 4, 2022 and reviews were received on July 5, 2022. Revisions were submitted on August 8, 2022 and the manuscript in its present form was accepted for publication on August 11, 2022. This preprint is posted online in accordance with GSA's Green Open Access policy. Note that minor changes have been made in the subsequent copy-editing process. The final version was published online on November 29, 2022, and can be accessed here: https://doi.org/10.1130/B36500.1

Please contact Theron Finley (tfinley@uvic.ca) for questions or feedback.

Modern Dextral Strain Controls Active Hydrothermal Systems in the Southeastern Canadian Cordillera

Theron D. Finley[1,2], Stephen T. Johnston[1], Martyn J. Unsworth[1,3], Jonathan Banks[1], Dinu-Ion Pana[4]

[1]Department of Earth & Atmospheric Sciences, 1-26 Earth Sciences Building, University of Alberta, Edmonton, Alberta, Canada

[2]School of Earth and Ocean Sciences, A405 Bob Wright Centre, University of Victoria, Victoria, British Columbia, Canada

[3]Department of Physics, 4-181 CCIS, University of Alberta, Edmonton, Alberta, Canada

[4]Alberta Energy Regulator/Alberta Geological Survey, 402 Twin Atria Building, 4999 – 98 Ave., Edmonton, Alberta, Canada

ABSTRACT

Thermal springs in the southeastern Canadian Cordillera occur in association with several major fault zones, which may permit deep circulation of fluid through fractured reservoirs to depths greater than 2 km. Both the current stress field and the most recent kinematics of these faults likely play a significant role in localizing hydrothermal upwellings but are poorly resolved. In this paper, we present new data from structural mapping along the Columbia River, Slocan Lake, Purcell Trench, Southern Rocky Mountain Trench, and Redwall faults. Fault plane and slickenfibre orientations measured in the field indicate a previously unidentified, post-Eocene phase of dextral strike-slip kinematics on these faults, which have historically been mapped primarily as Eocene extensional structures. The NE-SW maximum principal stress required for these kinematics shares a similar orientation to the present-day stress field derived from crustal earthquake focal mechanisms, which suggests dextral slip may be a recent and ongoing development that continues at the present time. On a regional scale, there is a positive correlation between the location of springs and regions with elevated seismicity. At the local scale, geothermal upwellings may be controlled by local zones of enhanced permeability including fault intersections and strain transfer zones. The identification of favourable structural settings may enable discovery of hidden (a.k.a. blind) geothermal energy resources.

1. INTRODUCTION

Active hydrothermal systems (i.e., thermal springs) in the Canadian Cordillera are broadly associated with major fault zones (Grasby and Hutcheon, 2001). These fault zones likely act as conduits

for deep circulation of meteoric water, however, the specific factors that localize thermal springs along these structures are poorly resolved, and the locations of potential blind geothermal systems (e.g., Craig et al., 2021) are difficult to predict. An improved understanding of the structural controls on these systems is necessary to encourage further geothermal development in Canada.

This paper is primarily concerned with the structural and tectonic controls on the location of these hydrothermal systems in southeastern British Columbia (BC), Canada. This region has anomalously high heat flow (Blackwell and Richards, 2004; Majorowicz and Grasby, 2010) and a high density of thermal springs compared to the rest of the Cordillera despite a notable absence of a magmatic heat source (Figure 1). It has been suggested that faults are the primary control on their location; Grasby and Hutcheon (2001) compared several parameters, including heat flow, permeability, topography/relief, infiltration rate, and the presence of fault zones, with regards to their influence on the location of thermal springs. Ultimately they determined that—with the exception of springs near the Pliocene to recent Mount Meager volcanic complex (Read, 1990)—fault zones act as a primary control on the position of thermal springs in the Canadian Cordillera, whereas the other factors have a negligible influence. Variations in crustal heat flow, precipitation/infiltration rate, and topographic relief were determined to occur on wavelengths of hundreds of kilometers, which are too broad to explain the pattern of hot spring occurrence. Specific fault-related parameters such as kinematics, fault age, and current strain have not yet been investigated. Why do thermal springs cluster in certain regions of the Cordillera, why do some faults host thermal springs while others do not, and why are thermal springs distributed unevenly along these fault zones? It is likely that inter- and intra-fault variations in geometry, kinematics, age, and permeability structure are critical controls on the localization of thermal springs. In addition to improving our understanding of known hydrothermal systems, answering these questions may also help identify hidden geothermal resources, also known as “blind” geothermal systems.

We focus on hydrogeologically-significant properties (kinematics, geometry, age and activity) of five faults zones in southeastern BC — the Columbia, Slocan, Purcell Trench, Southern Rocky Mountain Trench and Redwall faults — all of which are spatially associated with hydrothermal systems. Herein are presented new structural data that allow us to identify a previously undocumented phase of post-Eocene dextral strike-slip faulting. The data suggest that the post-Eocene reactivation of pre-existing Cordilleran structures provides a primary constraint on the localization of potential geothermal systems in southeastern BC. Our interpretations of the timing of deformation, structural controls on individual hydrothermal systems, and implications for regional tectonics are addressed in later Discussion subsections. First, we provide a brief overview of geothermal systems in the Canadian Cordillera and the importance of faults in controlling their location. Then, in the Study Area section, we summarize existing

research and knowledge about the five major fault systems studied in this paper before describing our methodology and new results.

1.1 Geothermal Systems in the Canadian Cordillera

The Canadian Cordillera is an ~800 km wide orogen that stretches from the Arctic Ocean to the United States border, mostly within the boundaries of Northwest Territories, Yukon, British Columbia, and Alberta. Its elevated topography, rugged relief and complex geology reflect a protracted and ongoing interaction between various oceanic plates, accreted terranes, and continental North America (Gabrielse and Yorath, 1991). The Cordillera is one of the most promising regions in Canada for geothermal energy development due to its high heat flow and elevated geothermal gradients (Grasby et al., 2012). Whereas much of eastern and central Canada is underlain by old and cold cratonic lithosphere and ancient orogenic belts, the Cordillera is geologically young and is subject to ongoing tectonic and magmatic processes that are conducive to the development of geothermal systems.

The geothermal gradient of the Cordillera ranges from 20 to 50°C/km . These values, though lower than most conventional high enthalpy geothermal energy resources, are similar to gradients measured in low enthalpy systems being explored and developed for electricity generation in Europe and New Zealand (e.g., Agemar et al., 2014; Reyes, 2015; Farquharson et al., 2016). Crustal heat flow in the Cordillera ranges from ~40 to 130 mW/m^2 (Hyndman and Lewis, 1995; Blackwell and Richards, 2004; Majorowicz and Grasby, 2010). Heat flow is locally very high (>200 mW/m^2) near active volcanoes in the Garibaldi volcanic belt in southwestern BC (e.g., Mount Meager), but these values do not reflect the bulk thermal conditions in the Cordillera. In several broad regions heat flow exceeds 100 mW/m^2 (see Majorowicz and Grasby, 2010), which is comparable to geothermal energy–producing regions such as Nevada and Utah (Blackwell and Richards, 2004).

The presence of more than 130 thermal springs throughout the Cordillera (Figure 1) provides a first-order indication that heat flow might be sufficient for geothermal energy extraction. Outlet temperatures of these springs range from 20 to 80°C (Woodsworth and Woodsworth, 2014). Aqueous geothermometers, which estimate reservoir temperature based on solute concentrations and ratios at the spring outlets, indicate that the maximum temperatures reached by some of these systems exceeds 180°C, implying maximum circulation depths in the range of 2–5 km based on the regional geothermal gradient (Grasby and Hutcheon, 2001; Allen et al., 2006, p. 20; Caron et al., 2007; Grasby et al., 2019). Although thermal springs are not necessarily the best indicator of geothermal prospectivity (Ferguson and Grasby, 2011), they do provide a basic indication of geothermal resource potential, in a subsurface environment that is otherwise poorly constrained by data.

1.2 Fault Zones and Their Relation to Hydrothermal Systems.

Fault zones play a critical role in directing groundwater flow due to their anisotropic permeability structure and are therefore key controls on the localization of hydrothermal systems. Typically, cross-fault flow is impeded by the impermeable, clay-rich fault core material, while along-fault flow is facilitated by the permeable, fractured, damage zone (Caine et al., 1996). A common conceptual understanding of thermal spring circulation cells is that meteoric water percolates down through the crust until it encounters a fault, along which it can rapidly ascend towards the surface (Grasby and Hutcheon, 2001; Menzies et al., 2016; Grasby et al., 2019). Faults often crop out in valleys or at slope-breaks at mountain fronts due to accelerated erosion of comminuted fault rock, or differential erosion between hanging wall and footwall As a result, there is a natural topographic drive to fault-controlled hydrothermal systems, with recharge occurring in mountainous highlands.

There are several factors that influence the permeability of fault zones, including their age, kinematics, and stress state. It has been shown in other structurally-controlled geothermal systems that the current stress state of the crust and resulting fault kinematics can predict which fault segments are the most permeable; faults oriented parallel or oblique to S_{Hmax} (maximum horizontal compression) are more likely to be permeable because of their tendency to dilate or slip, respectively, whereas those oriented perpendicular to S_{Hmax} are more likely to remain sealed (Barton et al., 1995; Meixner et al., 2016). Furthermore, there is a positive correlation between strain rate and fault permeability: seismic activity has been shown to maintain fault permeability via episodic refracturing of minerals precipitating within the fault zone (Curewitz and Karson, 1997; Faulds et al., 2012). Within seismically active regions, specific structural settings have been shown to be especially favourable to hydrothermal upwelling. Sibson (1996) showed that in fault-fracture “meshes”, high structural permeability develops parallel to fault-fracture intersections (often parallel to σ_2, the intermediate stress axis). Curewitz and Karson (1997) reviewed 25 hydrothermal fields around the world and suggested that stress concentration at fault tips, fault interaction zones (releasing and restraining bends), and fault intersections promoted long-lived fracture permeability and therefore hydrothermal upwelling. In the highly structurally-controlled geothermal fields of the Great Basin in Nevada, Faulds and Hinz (2015) categorized the structural settings of 426 geothermal systems and found that zones of greater structural complexity (e.g., relay ramps, step-overs, fault terminations, fault intersections, etc.) host the majority of geothermal systems due to enhanced permeability across multiple fractures. Siler et al., (2018) tested this empirical relationship by modelling stress changes at step-overs and terminations resulting from Holocene fault slip at two geothermal fields in Nevada and found that the area of highest stress perturbations corresponded well to areas of greatest hydrothermal fluid flow. Based on this work, the locations of previously unidentified blind geothermal systems have been successfully predicted via detailed mapping and identification of favourable structural settings (e.g.,

Craig et al., 2021). A similar approach may be appropriate for the amagmatic, fault-associated hydrothermal systems in British Columbia.

2 STUDY AREA

2.1 The Columbia River Fault

The Columbia River fault extends ~225 km southward from the Mica hydroelectric dam on Kinbasket Lake (52°N) to Lower Arrow Lake south of Nakusp (50°N) (Figures 1 and 2). It is mapped as having a shallow eastward dip of 20-30° (Read and Brown, 1981). In the footwall to the west are amphibolite- to granulite-grade metamorphic rocks of the Monashee Complex, and in the hanging wall to the east are complexly deformed Neoproterozoic and Paleozoic sedimentary rocks intruded by Mesozoic plutons. Normal dip-slip displacements estimated on the basis of offset metamorphic isograds range between <1 km (Lemieux et al., 2003), 1–10 km (Lane, 1984), 15–80 km (Read and Brown, 1981) and 30 km (Parrish et al., 1988). Excavations during the construction of the Revelstoke hydroelectric dam (51°N) in the late 1970s provided the opportunity for detailed structural analysis of the brittle Columbia River fault; Lane (1984) measured the orientation of kinematic indicators at the dam site and at several sites north of the dam. He concluded that primary displacement was normal dip-slip in the Eocene, followed by a minor phase of dextral strike-slip motion. He also speculated that the right-stepping bend in the trace of the fault at the dam site might be associated with vertical axis rotation during dextral transpression.

Many of the thermal springs associated with the Columbia River fault occur in the vicinity of Nakusp (Figure 2). The commercially developed Halcyon spring discharges on the east shore of Upper Arrow Lake, along the mapped trace of the Columbia River fault (Kraft et al., 2011). Several springs—Upper and Lower Halfway, St. Leon, Nakusp (commercially developed), and Wilson Lake springs—issue from within or adjacent to the Jurassic Kuskanax batholith, which underlies most of the mountain range to the northeast of Nakusp (Parrish and Wheeler, 1983; Thompson et al., 2009b). Several warm springs—Snowshoe, Jorden Ranch, Octopus Creek, and Taylor springs—occur along the shores of Lower Arrow Lake south of Nakusp, along topographic lineaments that possibly represent the southern termination of the Columbia River fault (dashed red lines, Figure 2).

2.2 The Slocan Lake Fault

The Slocan Lake fault system extends ~110 km from Nakusp, south along Slocan Lake to Castlegar, where it is known as the Champion Lake fault (Corbett and Simony, 1984) (Figures 1 and 2). Although there are no known warm springs along the Slocan Lake fault, it is included in this study because of its possible kinematic link to the Columbia River fault. In the footwall to the west of the Slocan Lake fault, are the amphibolite- to granulite-grade metamorphic rocks of the Valhalla Metamorphic Complex. The hanging wall is dominantly composed of granodiorite of the Jurassic Nelson Batholith. Eocene-aged ductile and brittle normal shear in the central segment of the fault is thought to

reflect at least 10 km of normal slip (Carr, 1986; Parrish et al., 1988). Interpretations of deep seismic reflection profiles suggest that the fault zone dips moderately east, penetrating the Moho (Cook et al., 1992).

2.3 The Purcell Trench Fault

The Purcell Trench is a major valley that begins in northern Idaho and merges northward with the Southern Rocky Mountain Trench (SRMT) at 51°N for a total length of ~330 km (Figures 1 and 3). For much of its southern segment it is occupied by Kootenay Lake. A sharp east-west contrast in metamorphic grade across the southern trench has led some to map an east-side-down normal fault—the Purcell Trench fault—along its southern segment (Doughty and Price, 1999, 2000). Note that the Purcell Trench fault is confusingly not the same as the Purcell Thrust, which lies in the SRMT to the east. The Purcell Trench fault is mapped from northern Idaho (48.5°N) as far north as the town of Balfour at 49.5°N (Doughty and Price, 2000; Brown and MacLeod, 2011; Cui et al., 2017). Along the western shore of the northern reaches of Kootenay Lake, several west-dipping normal faults (including the Lakeshore fault, Figure 3) may have developed due to the same Eocene extension that caused the Purcell Trench fault (Moynihan and Pattison, 2008). At 51.25°N, the valley bifurcates into the NNW-trending Trout Lake and the N-trending Duncan Lake valleys. The Lakeshore-Schroeder fault parallels the western edge of the Trout Lake valley, and may merge with the east-side-down Adit fault (Thompson and Dhesi, 2009; Kraft et al., 2011). No extensional structures are mapped in the southern Duncan Lake valley for ~75 km northward. However, in the northern-most segment of this valley, the east-dipping Beaver River normal fault, which truncates the western boundary of the Dogtooth duplex near Golden, was mapped by Poulton and Simony (1980) and Kubli and Simony (1994).

The Purcell Trench hosts one major hot spring, located at Ainsworth (Figure 3). It discharges from calc-silicate rocks in the immediate footwall of the Lakeshore fault on the western side of central Kootenay Lake. Additionally, on the east side of the lake, warm water discharges in the subsurface of the Bluebell Mine at Riondel (Desrochers, 1992), and there is a warm spring in the Orebin Creek valley east of Crawford Bay (Woodsworth and Woodsworth, 2014).

2.4 The SRMT Fault

The SRMT constitutes the southern segment (800 km) of a nearly 3000 km long topographic lineament that stretches from northwestern Montana, through eastern British Columbia, across the Yukon Territory, ultimately terminating north of Fairbanks, Alaska (Figures 1, 4, and 5). The segments of this lineament in northern BC and Yukon are known as the Northern Rocky Mountain Trench and Tintina Trench, respectively, and these are known to host major Eocene dextral faults with a cumulative offset of 450 km (Roddick, 1967; Gabrielse, 1985; Pope and Sears, 1997; McMechan, 2000). The SRMT is instead occupied by a steeply west-dipping normal fault—the SRMT fault—for much of its length. A shallowly

west-dipping Cretaceous thrust fault, the previously discussed Purcell Thrust, crops out along the west wall of the SRMT.

Evidence for extensional displacement along the SRMT fault is documented near the town of Valemount, BC; McDonough and Simony (1988) noted a “crush zone” with west-side-down dip-slip slickenfibres on the northeast shore of Kinbasket Lake and estimated that it offsets the Paleoproterozoic gneisses of the Malton Gneiss Complex by less than 2 km. 100 km to the south, between the Solitude and Adamant ranges, Gal and Ghent (1990) proposed 2 km of west-side-down displacement to explain the apparently undisturbed metamorphic isograds; southwest-side-up movement on the post-metamorphic Purcell Thrust would have displaced the isograds, but normal dip-slip on the SRMT fault may have restored them to their approximate original positions. Fraser et al. (2021) used apatite low-temperature thermochronology to distinguish several phases of extension-related cooling, notably including 3.6 km of east-side-down displacement on the SRMT fault in the early- to mid-Miocene, which is at odds with previous assertions of Eocene west-side-down displacement (e.g., McDonough and Simony, 1988). Additionally, they found evidence for 1.3-2 km of west-side-down displacement on the SRMT fault from the late Miocene to present.

At the south end of Kinbasket Lake the SRMT widens considerably, and mapping has failed to identify any normal faults for a 150 km interval to the south. Instead, the Purcell Thrust, which places metamorphosed rocks from the west over unmetamorphosed rocks to the east (Kubli and Simony, 1994), is the main fault occupying the valley floor (Figures 1 and 5). At the south end of Kinbasket Lake the Beaver River normal fault diverges from the SRMT fault at a ~20° angle to the west (Figures 1 and 3); Poulton and Simony, 1980), occupying the floor of the northernmost Purcell Trench (see preceding section). An alternative suggestion is that the SRMT fault (variably mapped as the Chancellor fault, e.g., Gal and Ghent (1990)) diverges ~15° to the east, ultimately merging with the White River lineament of Henderson (1954) and North and Henderson (1954a, 1954b), which has variably been interpreted as a thrust fault, or dextral shear zone (Charlesworth, 1959).

In the southernmost part of the trench near Cranbrook, the distribution of Miocene sediments suggests that extensional block faulting occurred along the SRMT from the Eocene to Pliocene or younger (Clague, 1974). Seismic reflection profiles and balanced cross sections at this latitude (49-54 °N) indicate at least 10 km of down-to-the-west dip-slip offset across the SRMT fault (Höy, 1993; van der Velden and Cook, 1996).

The segment of the SRMT near Valemount is moderately seismically active. Purba et al. (2021) deployed a temporary array of seismometers to identify 47 small earthquakes over a period of a year in the vicinity of Valemount. In the past few decades, several notable earthquakes have occurred on or near the trace of the SRMT, including a M 4.8 event on the east side of Kinbasket Lake (Rogers et al., 1980)

and a M 6.1 near the present location of the Mica hydroelectric dam (Rogers and Ellis, 1979). There is a growing body of evidence of recent earthquake activity along strike to the north and south as well (Rogers et al., 1990; McClymont et al., 2016; Finley et al., 2021).

Eight thermal springs occur in the vicinity of the SRMT. Three occur directly along the SRMT fault, while the remaining five occur along the parallel Redwall and Lussier faults. Thirty kilometers south of Valemount, the Canoe River spring discharges on the southwestern shore of Kinbasket Lake (Figures 1 and 4) near the intersection of a splay and the main strand of the SRMT fault (McDonough and Morrison, 1990; Jess et al., 2021). South of the Canoe River spring there is a 270 km segment of the trench where no springs occur. This gap roughly corresponds to the segment of the trench where the valley floor is occupied by the Purcell Thrust. At the south end of this gap, the Wolfenden warm spring occurs along the floor of the trench near the hamlet of Spillimacheen (Figure 5). The Fairmont spring occurs along the main trench valley, and although no faults are mapped at its location, the SRMT fault projects underneath thick Quaternary cover towards its location.

2.5 The Redwall and Lussier River Faults

The Radium and Red Rock springs are closely associated with the Redwall fault, while the Lussier, Ram Creek, and Wildhorse springs occur along the Lussier River fault. Both of these faults lie parallel to and 10-20 km to the east of the SRMT (Figures 1 and 5).

The Redwall fault is an enigmatic structure that has not been investigated in great detail since it was first mapped by Henderson (1954). Its surface trace extends from north of Radium, south along the Stanford Range of the eastern Rockies, intersecting the Kootenay River at the Red Rock warm springs, before its surface trace is lost 40 km north of Cranbrook. It has been suggested that it merges with the Lussier River fault to the south (Foo, 1979), which also hosts several thermal springs. The fault is subvertical for its entire length, leading several authors to conclude that it originated as a strike-slip fault characterized by either sinistral (Henderson, 1954) or dextral (Charlesworth, 1959) motion. Alternatively, Foo (1979) considered the Redwall fault to be a back-rotated thrust fault.

The Redwall fault is so-named due to the striking red colour of the fault zone, caused by hematite oxidation. The fault zone occurs in conjunction with a zone of subangular to subrounded, matrix-supported pebble to boulder conglomerate. This texture was originally interpreted to represent a zone of Cretaceous fault breccia (Henderson, 1954), but subsequent investigations have suggested that most of the breccia may be due to pre-Cretaceous evaporite-solution collapse (e.g., Stanton, 1966), a theory supported by the proximity of extensive gypsum deposits (Henderson, 1954). Stratigraphic offsets, and evidence of shearing within the solution-collapse breccia, indicate that it has subsequently been reworked by faulting (of hitherto uncertain kinematics), with strain concentration possibly occurring in the rheologically-weak

evaporites. The unique geological conditions of the Redwall fault, and their possible influence on hydrogeology are discussed later.

2.6 Summary of existing knowledge on faults studied

In summary, faults associated with the SRMT, Purcell Trench, and Columbia River valleys, are all known to have accommodated Eocene ductile and brittle extension. Estimates of offset on individual structures vary widely between 1-80 km. In most cases, the magnitude and kinematics of slip has been estimated by recognizing offset strata and metamorphic zones rather than through detailed kinematic analysis of the fault zones themselves. While many of the Eocene normal faults in southeastern BC are steeply dipping and brittle, a few have very shallow dips and ductile kinematic indicators (e.g., Columbia River and Slocan Lake faults). Little attention has been paid to the post-Eocene kinematics and activity of these faults, which is arguably the most consequential time period when considering structural permeability and hydrothermal activity. Eocene extension is generally held to be the most recent phase of deformation, but the results presented herein demonstrate otherwise.

3 METHODS

Detailed structural fieldwork was conducted in the summers of 2018 and 2019 over nine weeks in the triangular region between Valemount, Castlegar, and Fernie (Figure 1). Exposures of previously studied brittle faults were specifically targeted and many newly documented outcrops and fault exposures were visited. Georeferenced geological maps were used to locate exposures of faults mapped by previous workers. Work focused on road- and highway-side outcrops, and on lake shorelines where kinematic indicators were most likely to be exposed on fresh surfaces. In many places the principal fault planes are inferred to run along valley bottoms, covered by lakes and Quaternary sediment. Therefore, the fault planes measured in this study are mostly considered to be parallel splays that can act as proxies for determining the kinematics of the main fault.

Representative measurements were made of all significant observable sets of kinematic indicators at each outcrop. Photographs were taken of significant, well-exposed fault planes and kinematic indicators (Figures 6-9). Cross-cutting relationships (see annotated photographs in Figures 6 and 7) and regional relations (as reviewed in the Discussion) were used to constrain the relative timing of deformation. Slickenfibres – where mineral growth (quartz and/or calcite) occurs on the lee side of fault plane asperities – were considered to be the highest confidence kinematic indicator and represent the majority of our dataset. Care was taken to avoid mistaking Riedel shears and other ambiguous kinematic indicators for the more diagnostic mineral (quartz and/or calcite) growths on the lee side of fault plane asperities (Petit, 1987, Doblas, 1998). Slickenfibres and other kinematic indicators were ranked on a relative confidence scale of 1-3, where 1 indicated an ambiguous sense of slip, 2 indicated a preferred, but not certain, sense of slip and 3 indicated an unequivocal sense of slip. Those with rankings of 1 were

excluded from kinematic analyses but included in statistics of fault dips and slickenfibre/slickenline plunges. Slickfibre measurements are only useful if there is confidence that they represent a major tectonic episode, and that they have not been deformed (folded) by subsequent tectonism. Therefore, kinematic indicators were not measured if the fault plane did not visibly crosscut the entire outcrop, or if the fault plane was curved. This selectivity ensured that extraneous noise in the data was reduced. The potential for bias towards measuring fault planes striking parallel to road segments was recognized and addressed in the field: we ensured that each outcrop was thoroughly inspected for less-obvious fault planes striking at high angles to the road with smaller visible planes. In total 662 orientation measurements of fault planes, slickenfibres, and other kinematic indicators were collected (see supplemental material for the full data set). Due to the scatter inherent to structural orientations collected over such a broad region, the measurements were subdivided on the basis of geographic location, orientation, and kinematics, to illustrate the trends and clusters more clearly.

Irrespective of location, all fault plane measurements were plotted on rose diagrams (circular histograms) to show the overall trends in strike and dip (Figure 10a and b). The kinematics for each measurement were further categorized according to slickenfibre rake (sinistral=0°, dextral=180°, normal=-90°, reverse=+90°), and plotted on a rose diagram to represent the relative proportions of each group (Figure 10c). Finally, all measurements were plotted on a moment triangle (Frohlich, 1992) to demonstrate the kinematic populations present in the entire dataset (Figure 10d).

Fault plane measurements were also divided by location: measurements from the Columbia River, Slocan Lake, Purcell Trench, SRMT and Redwall faults were separated to investigate any variation in kinematics between each major structure (Figure 11). Measurements in each fault zone were filtered based on the regional trend of each fault-occupied valley. Because each valley is already known to host a major fault, it is reasonable to assume that most significant faults strike parallel the valley trend regardless of their kinematics; this assumption is supported by the fact that the majority of kinematic indicators collected in this study record strike-slip and normal dip-slip on fault planes parallel to the valleys. A threshold value of 30° to the average valley trend was used so as to capture most fault strands that fall within the possible range of R and P shears (which would ideally be oriented 15° to the main fault occupying the valley; Dresen, 1991), and to exclude any potential antithetic R' and P' shears (which would ideally be oriented 75° to the valley). The valley-parallel filtered data were then divided into groups based on their kinematics (dextral, normal, etc.). The unfiltered and filtered datasets are shown in Figure 11. Data were also divided into local clusters collected within a maximum radius of 10 km to display local variation within fault zones. These locally clustered data accompany maps in Figures 2-5.

All groups of structural measurements were plotted on equal-area lower-hemisphere stereonets (shown in Figures 2-11) and analyzed using the Orient software package developed by Vollmer (2019).

Angular misfits between the measured fault plane and slickenfibre pairs provided an indication of data quality, and those with misfits greater than 20° were discarded. Misfits were not artificially corrected by rotating the slickenline into parallel with the fault plane, as this procedure did not significantly affect the results of the subsequent kinematic analysis and doing so would obfuscate real error in the data. Beachball plots and accompanying P (compressional), M (intermediate), and T (tensional) axes were calculated from the average kinematics of each set of structural measurements. On these plots, the black great circles illustrate the strike and dip of fault planes, and the red dots show the trend and plunge of slickenfibres. The white and grey quadrants of the beachballs indicate the average orientation of P and T axes respectively Because the P-, M-, and T-axes of fault plane solutions can be poor approximations for principal stress axes (σ_1, σ_2, and σ_3) as demonstrated by McKenzie (1969) we also performed a formal stress inversion (Angelier, 1984; Célérier et al., 2012) to estimate the stress tensors for our sets of fault plane measurements.. This method searches for the best fitting stress tensor by minimizing the misfits between the resolved shear traction and the measured slip directions in a population of faults. The method does not determine the absolute magnitudes of the principal stresses, just the orientation and relative dimensions (Bishop's ratio) of the stress tensor. Bishop's ratio is given by:

$$B = \frac{\sigma_2 - \sigma_3}{\sigma_1 - \sigma_3}$$

The software performs a grid search for the best fit, iterating by increments of 2° through 1024 grid nodes, and increments of 0.01 for Bishop's ratio (between -1 and 1). Goodness of fit (d_i) is defined as the dot product between the fault slip and the resolved shear stress, and ranges between 1 (parallel, perfect fit) and -1 (antiparallel). For N faults (where w is an optional weighting factor) the fit of each stress tensor (D) is defined as:

$$D = \frac{1}{N_w} \sum_{i=1}^{N} d_i w_i$$

The results of the stress inversion are compared with the P-, M-, and T- axes in Figure 11.

4 NEW RESULTS AND OBSERVATIONS

Our dataset of brittle fault kinematic indicators provides evidence for widespread dextral strike-slip on the three major fault systems in southeastern BC. Of the 662 fault-slickenfibre pairs we collected, 42.6% indicate dextral and dextral-oblique slip, 24.9% indicate pure normal slip, 21.5% indicate sinistral and sinistral-oblique slip, 6.6% indicate reverse, and the remainder (4.4%) are ambiguous. A full table of fault plane and kinematic indicator orientations is provided in the supplemental material. When plotted according to rake and on a moment triangle (Figure 10c,d), two distinct populations emerge: dextral and normal. Most fault planes measured in the field were minor and did not have broad damage zones or

mature clay gouge, which suggests that they represent minor splays of larger faults assumed to be beneath lakes and glacial overburden in valley bottoms. Where large fault zones with broad zones of breccia and gouge were observed, they were most commonly dextral. Of the sinistral fault planes, 54.9% strike at high angles (>30°) to the strike of the fault-occupied valleys in which they lie. Among the faults oriented at low angles (<30°) to the strike of the valleys, distinct populations of normal and dextral kinematic indicators emerge (Figure 11). The mean orientation of the dextral fault population is subparallel to the mean orientation of the normal fault population (Figure 11). While many of these fault zones have previously been interpreted to have undergone Eocene normal displacement on planes with dips ranging from steep to shallow (Parrish et al., 1988), our observations indicate that these kinematic indicators occur predominantly on subvertical to vertical fault planes: 71% of the fault planes observed dip steeper than 60° (Figure 10b).Below, we review the observations from key sites in the study area, as well as stress inversion results from all subsets of data The similarity of our results across multiple fault planes over 100s of kilometers suggest that there has been little or no subsequent tectonic disturbance of these structures.

4.1 The Columbia River Fault

Detailed fieldwork along the Columbia River fault revealed abundant brittle dextral kinematic indicators on sub-vertical fault planes. In this section, significant outcrops are described from north to south, from the Mica hydroelectric dam to the Nakusp region on Upper Arrow Lake. The spatial distribution of kinematics measured in the field are illustrated in Figure 2 and annotated field photos are shown in Figure 6.

Immediately south of the Mica Dam, a consistent set of north-northwest dipping normal faults (Figure 6a) are exposed where the valley makes an abrupt change from a west-southwest orientation to a southeast trend, perhaps marking a releasing bend in a northwest-southeast striking dextral-system. At the eastern abutment of the Revelstoke Dam, both normal and dextral kinematic indicators were observed in a broad zone of gouge and fault breccia believed to be a hanging-wall splay of the main Columbia River Fault zone now buried beneath the dam (Figure 6b). Fault planes here mostly dip steeply (>60°) to the east and southeast, and slickenfibres trend from south to southwest. These measurements are consistent with those of Lane (1984) at this site, who concluded that the dextral motion post-dated the Eocene dip-slip component. Other exposures (Hathaway Ck. and Carnes Ck.) documented by Lane (1984) were revisited, but few diagnostic slickenfibres were observed.

Forty kilometers south of Revelstoke, near the Shelter Bay ferry terminal on Upper Arrow Lake (Figure 2), a near-vertical, north-striking, 50 cm wide fault gouge zone cuts through granodiorite of the Upper Jurassic (~160 Ma; Parrish et al., 1988) Galena Bay stock. Horizontal slickenfibres with

ambiguous slip sense were observed on the fault walls, but potential Riedel shears oriented ~15° to the main fault plane are consistent with dextral slip.

Thirty kilometers north of Nakusp, Highway 23 follows the trace of a NNW striking fault plane with dextral and sinistral slickenfibres on vertical planar surfaces on either side of the road. Another fault, with a 1-2 m wide gouge zone cuts across the outcrop towards the NE (Figure 6c). Dextral slickenfibres are present on its walls. This fault zone appears to be aligned with the Blind Bay fault mapped by Kraft (2013). The 60° angle between these two faults suggests they may be a conjugate pair.

West across Upper Arrow Lake from Nakusp is an outcrop of fault gouge that was originally interpreted by Lemieux et al., 2003 as an exposure of the locally northwestward-striking, northeast-dipping Columbia River fault. The main schistose fabric of the footwall rock was observed to strike west, and is deformed into small-amplitude south-verging folds. Such deformation is consistent with reverse faulting and crustal shortening along a northwest-striking restraining bend within an overall north-south striking fault zone, rather than east-west extension as postulated by Lemieux et al. (2003). We made a similar reinterpretation at an outcrop 10 km to the WNW near Arrow Park Lake (Figure 6d) that was previously mapped as a normal fault by Thompson et al., 2004b.

The southern tip of the Columbia River fault is commonly mapped as being east of the hamlet of Burton. However, the strong north-south topographic lineaments of Lower Arrow Lake (dashed lines, Figure 2) suggest that splays of this fault zone may continue southward from the left-stepping bend in the Columbia River fault west of Nakusp. One such lineament trends towards Burton, and an outcrop aligned with this lineament on the east side of Lower Arrow Lake hosts dextral slickenfibres on a steeply-dipping fault plane (Figure 6f). The second lineament follows the Whatshan valley towards the hamlet of Fauquier, where dextral slickenfibres were observed on fault planes in the Cretaceous (77-79 Ma; Thompson et al., 2004a, 2009a) Whatshan Lake batholith.

The Jurassic Kuskanax batholith, from which several thermal springs issue, has several north-south-striking faults mapped through its core, which appear to be subvertical based on their intersection with topography (Figure 2). Thompson et al. (2009b) mapped these faults as dextrally offsetting roof pendants of Paleozoic metavolcanic rocks as well as the surrounding Jurassic quartz monzonite. We documented vertical fault planes with dextral slickenfibres in exposures of the Kuskanax Batholith along the Halfway River (near Lower Halfway hot spring), and along Kuskanax Creek, 5 km west of Nakusp hot spring. It is likely that these faults arose from the same transpression that caused dextral motion on the Columbia River fault and may provide the permeability allowing hot springs to reach the surface within the batholith.

As shown in column 2 of Figure 11, of the 231 fault planes measured along the Columbia River valley from the Mica Dam to south of Fauquier, 160 (69%) are within 30° of the valley trend. Of these, 55

(34%) are dextral, while 60 (38%) are normal, while the remainder (28%) are a mix of sinistral (32), reverse (5), and ambiguous (8). Notably, a large portion of the valley-parallel sinistral and normal faults were from the Albert Point area, immediately south of the Galena Bay ferry terminal. The kinematics in this region are variable, and not as coherent as other segments of the valley. If kinematics from Albert Point are excluded from the analysis, valley-parallel fault kinematics are comprised of 42% dextral, 31% normal, 17% sinistral, 4% reverse, and 6% ambiguous). Of the 71 faults measured at high angle to the Columbia River valley, 28 (39%) were sinistral, 18 (25%) dextral, 16 (23%) normal, 8 (13%) reverse, and one ambiguous. Note that the high-angle sinistral faults share a similar P-axis orientation as the valley-parallel dextral faults, suggesting these populations are genetically related as conjugate sets.

4.2 The Slocan Lake Fault

In the region between southern Upper Arrow Lake and northern Slocan Lake, a belt of east-west-trending faults and folds (the Slocan Syncline; Ross and Kellerhals, 1968) occurs at a high angle to the regional strike (Parrish, 1981; Figure 2). Cretaceous and Cenozoic intrusions are affected by this deformation: brittle faults are observed on the margins of plutons, and felsic sills that intruded along the primary cleavage planes are folded, forming south-verging folds (Figure 6g). Age constraints on these intrusions are sparse, so it is difficult to confirm the timing of this deformation, but it is at least post-Cretaceous, if not post-Eocene. The north-south shortening in this region suggests that the region between the northern tip of the Slocan Lake fault and the southern tip of the Columbia River fault could be a restraining bend in a dextral system.

At two locations along the east side of Slocan Lake (Figure 2), where the Slocan Lake fault is exposed along Highway 6, sub-horizontal dextral slickenfibres were observed on subvertical fault planes, in one case on a brittle fault that cuts through the Eocene-aged Ladybird granite (Carr, 1992), and on another that cuts at a high angle (Figure 6h) across the Eocene-aged ductile fabric of the Valkyr shear zone (Carr et al., 1987). The Ladybird granite and Valkyr shear zone are well studied, and their ages well constrained to the Eocene. Thus, these cross-cutting relationships provide a critical lower age constraint on our post-Eocene strike-slip faulting.

As shown in column 3 of Figure 11, of the 23 fault planes measured along the Slocan Lake valley, 16 (70%) are valley parallel, and 12 (52%) of those are dextral. Of the remaining 7 (30%) at high angles to the valley, 3 are sinistral, 2 are dextral, and 2 are reverse.

4.3 The Purcell Trench Faults

Fieldwork revealed abundant brittle dextral kinematic indicators on subvertical fault planes along much of the Purcell Trench, Duncan River, and Trout Lake/Lardeau River valleys.The spatial distribution of kinematics measured in the field are illustrated in Figure 3 and annotated field photos are shown in Figure 7.

Five kilometers southeast of Beaton Arm on Upper Arrow Lake, an outcrop coincident with the mapped trace of the Adit fault – mapped as a west-side-down normal fault by Kraft et al. (2011) – hosts a 60 cm-wide vertical zone of oxidized breccia and gouge material (Figure 7a). Unambiguous dextral slickenfibres occur on the fault walls and cleavage appears to be locally dragged into parallel with the fault plane. Farther south along the Trout Lake valley, several outcrops host faint dextral slickenfibres on vertical planar surfaces. No fault has been mapped along the Lardeau River; the Adit fault diverges from the valley and is mapped in the mountains to the southwest. However, slickenfibres are consistently exposed at outcrops along the floor of this valley. At the south end of Duncan Lake, well developed dextral slickenfibres are present on a well-exposed fault plane in Cambrian Badshot Formation marble.

North along Duncan Lake and Duncan River, several outcrops display dextral slickenfibres (Figure 7b and c). This topographic lineament continues northward into the Beaver River valley, which merges with the Rocky Mountain Trench at 51.5°N. The steeply-west-dipping Beaver River normal fault is mapped in the northern end of this valley (Poulton and Simony, 1980; Kubli and Simony, 1994). It is possible that the valley is host to a through-going fault with a history of both normal and dextral slip.

Several locations within Cretaceous plutons on the east side of Kootenay Lake display vertical brittle fractures with dextral kinematics. On the west side of Kootenay Lake, just south of Kaslo, a well-exposed limonitic fault plane with faint dextral slickenfibres cuts obliquely through a highway outcrop (Figure 7d and e). On the west side of the Purcell Trench near Creston, Brown et al. (1994) documented a brittle fault zone which they interpreted to be a footwall splay of the Purcell Trench fault. Near this location, we found dextral slickenfibres on a notable vertical fault plane striking at a low angle to the main trench axis. Critically, this dextral fault appears to cross-cut and offset a normal fault in the same outcrop (Figure 7f), which suggests dextral faulting post-dates normal faulting.

As shown in column 3 of Figure 11, of the 224 fault planes measured within the Purcell Trench (including within the Duncan and Trout lake valleys), 160 (71%) are within 30° of the valley trend. Of those, 88 (55%) exhibit dextral kinematics, 44 (28%) are normal, and the remainder (17%) are a mix of sinistral, reverse, and ambiguous kinematics. Of the 65 fault planes that are oriented at high angle, 28 (43%) are sinistral, 22 (34%) are dextral, 14 (22%) are normal, and one is ambiguous. Note that the high-angle sinistral faults share the same P-axis orientation as the valley-parallel dextral faults, suggesting these populations are genetically related conjugate sets.

4.4 The SRMT Fault

Detailed fieldwork in the Valemount area in 2018 revealed abundant brittle dextral kinematic indicators on subvertical fault planes along Canoe Reach(the northern arm of Kinbasket Lake).The spatial distribution of kinematics measured in the field are illustrated in Figure 4 and annotated field photos are shown in Figure 8.

The kinematic indicators observed in this study are all related to brittle faulting, and are distinct from the Mesozoic mylonites documented along Kinbasket Lake by Murphy (1990) and the orogen parallel L-tectonites that define the Valemount Strain Zone immediately northeast of the SRMT (McDonough and Simony, 1989). The west-side-down "crush zone" at the north end of the lake documented by McDonough and Simony (1988) was observed, but these kinematics were not found to characterize other outcrops further south along the lake. As shown in column 5 of Figure 11, of the 152 fault planes and kinematic indicators measured in the Valemount area, 126 (83%) are subparallel (<30°) to the valley trend, and 64 (51%) of those indicate dextral slip while only 39 (31%) indicate normal slip. The remaining 23 (18%) valley-parallel fault planes (not shown in figure) host a mix of sinistral, reverse, and ambiguous kinematics. A total of 26 fault planes occur at high angles to the valley, and 19 (73%) of these are sinistral. Note that P-axes predicted by both the valley-parallel dextral faults and high-angle sinistral faults are similar, suggesting these populations are genetically related conjugate sets.

Two hundred kilometers south of Valemount (50 km north of Golden) near the southern end of Kinbasket Lake (Figure 3), an outcrop of Cambrian McKay Group in the immediate footwall of the Purcell Thrust fault displays abundant dextral slickenfibres on vertical fault planes (Figure 9c). Notably, these dextral kinematic indicators are nearly 200 km farther south than had previously been documented in the SRMT by Murphy (1990) and McMechan (2000).

4.5 The Redwall Fault

Dextral kinematic indicators were observed at exposures of the Redwall fault immediately east of Radium Hot Springs, along the Westroc mine road east of Invermere, and at the Red Rock warm springs on the Kootenay River forest service road east of Canal Flats.The spatial distribution of kinematics measured in the field are illustrated in Figure 5 and annotated field photos are shown in Figure 9.

An outcrop on a forest service road southwest of Lussier Hot Springs displays red- and orange-stained microbreccia and abundant slickenfibres characteristic of the Redwall fault, which is not traditionally mapped this far south. Dextral kinematic indicators were also observed on a fault plane assumed to be a splay of the Lussier River fault (Figure 9b), indicating that dextral shear is distributed throughout the eastern side of the SRMT. As shown in column 4 of Figure 11, of the 32 fault planes measured along the southern portions of the trench, 28 (88%) are within 30° of the valley trend, and 17 (61%) of these demonstrate clear dextral slip while the remainder host a mix of normal, sinistral, and ambiguous kinematics. Only 4 fault planes were measured at high angles to the valley and they are a mix of dextral and reverse.

4.6 Stress inversion results

Stress inversions performed on all subsets of kinematic data reveal consistent trends throughout the study area (Figure 11). Numerical results are provided in Table 1. In most cases, P-, M-, and T- axes are

good approximations for the principal stress axes. Generally, σ_1 plunges shallowly NE or SW, σ_2 is subvertical, and σ_3 plunges shallowly NW or SE. For the normal-parallel subsets, σ_1 is subvertical, and σ_2 and σ_3 plunge shallowly in variable directions. The filtered subsets of kinematic data (dextral-parallel, normal-parallel, and sinistral-high angle) have better fitting stress tensors than the un-filtered datasets (Table 1), indicating that each subset internally corresponds to a unique deformation event, whereas the unfiltered sets are comprised of multiple generations of strain.

5 DISCUSSION

5.1 Fault Kinematics and Age

Our data demonstrate that dextral faulting is the dominant mode of kinematics measured along the three major fault zones of the southeastern Canadian Cordillera. For the following reasons, it is likely that this phase of slip is the most recent and overprints other phases:

1. Dextral kinematic indicators observed on valley-parallel fault planes represent the largest population of all kinematic indicators (34%) (Figures 10 and 11). We make the assumption that older slip surfaces are more likely to have been overprinted and thus are less well represented in the data.
2. In several places, brittle dextral kinematic indicators occur near or overprint zones of late Cretaceous to Eocene ductile deformation (e.g., mylonites in the Columbia River fault and Slocan Lake fault (Figure 6), SRMT fault near Valemount (Figure 4)). Mylonites record shear strain from deeper structural levels below the brittle-plastic transition at ~15 km depth, whereas slickenlines and slickenfibres develop in brittle crust (Fossen and Cavalcante, 2017). Therefore, slickenfibres co-occurring with mylonites are likely the younger phase.
3. In several places, dextral kinematic indicators occur within Cretaceous plutons, and in one case within an Eocene pluton (Ladybird Granite), and therefore must postdate these intrusions, allowing for the cooling and exhumation of the plutons (Figure 2 and 3).
4. The regional stress orientations calculated from modern earthquake focal mechanisms (Ristau et al., 2007; Heidbach et al., 2018) are consistent with the average orientation of P-axes and principal stress axes determined for dextral fault plane-slickenfibre pairs in our study area (Figures 12 and 13), suggesting that this state of stress persists into the present day.
5. Brittle normal faults represent the second largest percentage of all kinematic indicators observed in the study area, and the majority of these faults share a similar strike and dip to the dextral faults (Figures 10 and 11). This suggests they are oriented favourably for dextral-reactivation in the post-Eocene stress regime defined by Ristau et al. (2007).

6. A notable population of sinistral faults oriented ~60° to the main population of dextral faults (Figure 11) is likely a genetically related conjugate set consistent with the NE-SW P-axes and σ_1 predicted by the dominant dextral phase.

5.2 Estimates of Magnitude of Offset

The amount of dextral offset across these multiple structures is difficult to estimate but is likely on the order of tens of kilometers based on the evidence provided below. Larger estimates of displacement on the order of hundreds of kilometers would ignore numerous cross-fault stratigraphic and magmatic (plutonic) correlations. Here, we discuss the constraints on offsets across each major fault zone:

Along the SRMT near Valemount (Figure 4), McDonough and Simony (1988) asserted that the textural, structural, and metamorphic similarities between the Malton Gneiss to the west and Yellowjacket and Bulldog Gneisses to the east precludes major dextral offset as suggested by (Chamberlain et al., 1985); we agree that it would be fortuitous for such similar packages of rock to end up adjacent to one another given that no other similar lithologies are cross cut by the SRMT fault to the north or south. Murphy (1990), referring to the dextral mylonites he observed along Kinbasket Lake, suggested that 55 km of late Mesozoic dextral displacement was possible based on a mapped offset of the Purcell Thrust fault and a staurolite-kyanite isograd. We agree with this maximum estimate of offset but argue that at least part of that offset was achieved during post-Eocene dextral slip. Farther south along the SRMT there are few stratigraphic horizons or identifiable structural boundaries to act as reliable piercing points. The trench lies parallel to the structural grain of the Foreland Belt, bounding the Proterozoic Purcell and Windermere Supergroups to the west and the Cambrian McKay Group to the east. A block of Purcell rocks crop out on the east side of the trench northeast of Cranbrook, but these could plausibly be restored to any position along the Purcell Anticlinorium for hundreds of kilometers northward along the trench.

Along the Purcell Trench north of Creston, the Late Cretaceous Bayonne batholith is mapped on both sides of the valley (Figure 3). Its north-south extent on the west side of the valley is nearly double that of the east side, allowing for the possibility of ~25 km of dextral displacement. K/Ar ages reported by Archibald et al. (1983) (also see: "Canadian Geochronology Knowledgebase," 2013) within the Bayonne Batholith on the west side of the valley are consistently 20 Myr younger (Early Paleogene) than those on the east side of the lake (Late Cretaceous), suggesting at best a complex cooling history that may further complicate attempts to unravel the displacement history. On the northern margin of the Bayonne Batholith, the distinctive conglomerates of the Neoproterozoic Toby Formation (basal Windermere Supergroup) strike at 40° to the trench and are similarly dextrally offset by ~25 km (Figure 3). Farther north along Kootenay Lake there are no distinctive piercing points, and the highly lineated rocks of the Early Paleozoic Hamill and Lardeau groups that strike parallel to the valley effectively obscure any strike-parallel offsets.

At the southern end of the Columbia River fault, several en-echelon dextral offsets, each less than 2 km, are mapped across Jurassic and Cretaceous plutons. Based on similar truncated structural patterns Parrish (1981) suggested that there might be 15 km of dextral slip across the Rodd Creek fault (now known as the southern tip of the Columbia River fault) of Hyndman (1968) but did not favour this hypothesis because "the structure and metamorphic grade to the north of each of these areas are markedly different". To the north of Nakusp, small offsets of <250m are mapped across vertical faults within the Jurassic Kuskanax batholith. Farther north along the Columbia River valley, no distinctive piercing points have been observed.

The small magnitude of young dextral offset observed on all of these fault zones may be a contributing factor to enhanced structural permeability in southeastern BC. As fault displacement increases so too does the width of the central gouge zone (Shipton et al., 2006), which is typically composed of impermeable clay rather than permeable fractures. Furthermore, as faults mature, strain often becomes progressively more concentrated, transitioning from a diffuse fracture zone to a discrete through-going fault plane. As has been pointed out by several authors (e.g., Sibson, 1996; Curewitz and Karson, 1997; Faulds and Hinz, 2015), greater structural complexity and fracture density is more conducive to hydrothermal fluid flow.

5.3 Neotectonic Stress and Strain

In situ stress measurements in the southeastern Cordillera are sparse and those that do exist are derived from earthquake focal mechanisms (Heidbach et al., 2018). The southeastern Canadian Cordillera is characterized by a low level of seismicity as compared to the active convergent margin to the west, but at greater levels than the central intermontane region of British Columbia, and the stable foreland basin and craton to the east (Figure 12a; Ristau et al., 2007). Strain rates estimated from geodetic GNSS instruments range between 4-16 nanostrain/year (Mazzotti et al., 2011; Kreemer et al., 2014), though the instrument coverage is sparse east of the Cascade forearc and the sense (kinematics) of strain is not well resolved. Within the study area, ~25 earthquakes occur each year, and are between M_w 0-6 (Figure 12a). Ristau et al. (2007) calculated moment tensor solutions for earthquakes of M_w 4 and greater for all of western Canada (moment tensor solutions are typically not possible for magnitudes less than ~ M 4). Few earthquakes above the required threshold have occurred in the study area since the beginning of the catalogue in 1985, but all are dominantly strike-slip, with dextral nodal planes aligned with the major fault zones of the Cordillera, and sinistral nodal planes oriented at high angles to the regional strike (Figure 12b). Maximum principal stress (σ_1) orientations inferred from these focal mechanisms (Ristau et al., 2007) are sub-horizontal and trend NNE-SSW. The earthquake focal mechanisms and associated P-axes and stress axes are closely aligned with the stress axes determined from structural measurements described in this study (Figure 13). For example, in 1978, a M_w 4.8 earthquake occurred south of

Valemount (Rogers et al., 1980), and was initially investigated due to concerns over the filling of the Kinbasket Lake reservoir. The preferred focal mechanism for this earthquake was dominantly right lateral, with a reverse component, on a SSE striking fault plane (see focal mechanism in Figure 4). Ultimately it was concluded that the earthquake was not induced by the reservoir, but rather was attributed to "stresses associated with residual strain energy stored during the mountain building process" (Rogers et al., 1980). The orientation of the focal mechanism of the McNaughton Lake earthquake is similar to the orientation of fault planes and slickenfibres observed in the area (Figure 4) and was therefore likely not due to "residual strain" but ongoing dextral transpression. Focal mechanisms of similar dextral transpressional kinematics were also resolved for two small earthquakes detected by a temporary seismic array near Valemount (Purba et al., 2021) and for the 1986 Prince George earthquake (Rogers et al., 1990).

It is notoriously difficult to infer stress from kinematic indicators preserved in rocks, due to the possibility of multiple overprints, as well as syn- and post-deformation rotations. However, the coherence of our dataset across a large geographic area indicates that these kinematic indicators are recording at most two major tectonic episodes: extension followed by dextral strike-slip. We therefore suggest that the dextral faults observed in this study are manifestations of the same stress that drives the low levels of seismicity in this region (Figure 12b). Furthermore, this ongoing seismicity may be important in maintaining fault permeability and allowing for the occurrence of thermal springs in the southeastern Cordillera.

5.4 Fault Permeability and Spring Localization

At a regional scale, low levels of seismic activity in the southeastern Cordillera may be responsible for maintaining crustal fault permeability, thereby controlling the occurrence of thermal springs in the area. In the Cordillera, three main clusters of thermal springs—coastal BC, the southern Mackenzie Mountains, and southeastern BC—all correspond to regions of elevated seismicity as compared to central BC (Figure 12). Curewitz and Karson (1997) showed that active strain enhances structural permeability via episodic re-fracturing of fault zones and surrounding wall rock that would otherwise be clogged by hydrothermal mineral precipitation. Furthermore, faults and fractures that are critically stressed and oriented parallel to, or between 30-45° to, the maximum stress axis, will either dilate or slip, respectively, thus permitting the flow of fluid (Barton et al., 1995). In other geothermal fields, strain rate is considered a critical control on geothermal prospectivity (e.g., Faulds et al., 2012). While patterns of seismicity cannot be used to predict specific locations of thermal upwellings, they can explain regional distributions. Past efforts to characterize the fault and fracture permeability of the entire Cordillera with regard to geothermal prospectivity (Kimball, 2010) did not consider the variable seismic activity, and weighted the permeability of all faults equally. It is evident from the correlation between regions of elevated seismicity

and clusters of thermal springs, that active faulting may be a broad control on the occurrence of hydrothermal upwelling (Figure 12).

At more local scales, specific structural settings appear to localize thermal spring outlets. Curewitz and Karson (1997) and Siler et al., (2018) showed that stress concentration at fault tips, step-overs, and intersections promoted structural permeability. Faulds and Hinz (2015) showed that local regions of enhanced structural complexity (e.g., pull-aparts) are particularly favourable for hydrothermal upwelling. Sibson (1996) showed that in fractured rock meshes, fluid preferentially flows parallel to σ_2 along fault and fracture intersections. Therefore, assuming an Andersonian model of faulting (Anderson, 1905), fluid flow in a strike-slip regime would be preferentially vertical. As we have shown in this study, recent kinematics of the southeastern Canadian Cordillera are predominately strike-slip, and therefore most conducive to vertical fluid flow.

It is likely that a combination of these structural settings is required to explain the localization of thermal springs in the Canadian Cordillera within the broader pattern of active regional strain. We assign a structural setting to each spring system; these are summarized in Table 2 and Figure 13, and discussed in detail below. In some cases, specific fault intersections can be identified: the Canoe River spring (Figure 4 and 13) occurs at the intersection of the main strand and a splay of the SRMT fault (McDonough and Morrison, 1990; Jess et al., 2021) and the Halcyon and Wiskey Pt. springs (Figure 2 and 13) occurs near the intersection of the Columbia River fault and the Blind Bay fault (mapped by Kraft, 2013). In other cases, intersections between smaller splays and Riedel shears not identified in regional mapping, but apparent in the angular variation of dextral fault plane strikes measured in this study, may provide the main control on geothermal springs. The cluster of thermal springs north of Nakusp (Figure 2 and 13) occurs north of the restraining bend between the Columbia River fault and Slocan Lake fault, and south of the restraining bend between the Columbia River fault and Adit fault, and therefore falls within a “fault interaction zone” as per Curewitz and Karson, (1997), where stress is concentrated, leading to increased fracture permeability. An example of this enhanced fracture density is found in the numerous small-offset dextral faults that cut the Kuskanax Batholith. The cluster of warm springs (Snowshoe, Jorden Ranch, and Octopus) south of Nakusp (Figure 2 and 13) may be due to stress concentration at the tip of a previously unrecognized splay of the Columbia River fault that follows the Whatshan Lake lineament. The Ainsworth spring and the two warm springs (Riondel and Crawford Bay) on the east side of the lake (Figure 3 and 13) occur in a potential zone of strain transfer between the steeply-west-dipping Lakeshore fault, and the steeply-east-dipping Purcell Trench fault. The springs along the Redwall fault (Figure 5) do not fit as readily into a zone of potential stress concentration. Instead, it is likely that a combination of primary permeability of the solution collapse breccia, and secondary permeability of Cenozoic fractures, makes this structure such a prolific host of thermal springs.

The oxidation of conglomerate clasts and surrounding matrix material suggests that the Redwall fault has a protracted history of hydrothermal flow. For example, at Red Rock warm springs, a large, layered, tufa dome is situated at the top of the cliff on the north side of the Kootenay River. The dome is bisected by the cliff such that the interior is visible, and no thermal water presently flows. Another tufa deposit occurs a few kilometers to the east. It is evident that hydrothermal flow on the Redwall fault is ephemeral, and that thermal springs have migrated along it through time.

If active strain and seismicity is the primary control on spring location, it follows that seismicity through time might lead to spring re-location. Cordilleran hot springs have, however, proved relatively resilient to seismicity; Jess et al. (2021) used thermochronology to determine the lifespan of the Canoe River hot spring, and arrived at an estimate of 4-5 Myrs, which is considerably longer than the (roughly constrained) recurrence interval of significant crustal earthquakes along the SRMT (Rogers and Ellis, 1979; Rogers et al., 1980, 1990; Adams et al., 2019). Following the October 2012 Haida Gwaii Mw 7.8 earthquake, Grasby et al. (2019) documented the cessation and gradual return of discharge at the Gandll K'in Gwaay.yaay hot spring. That the spring water ultimately followed the same route to the surface following such a large and proximal event, further demonstrates the resilience of these fluid pathways to seismicity. A key question then, is what circumstances do lead to a shift in spring outlet, as apparently happened at the Red Rock warm spring. Finley et al. (2021) documented a possible Holocene fault scarp located 11 km northwest of the Red Rock spring, and 4 km due south of the Fairmont hot spring (Figure 5). Determining the influence of the seismic event responsible for this fault scarp on spring location will require more investigation. In the case of the Canoe River hot spring, Jess et al. (2021) suggest that the onset of spring discharge could be related to increased volcanism. While this may be true on a regional scale, it does not explain the exact location of the spring. The regional and local structural and seismic controls must also be considered.

5.5 Predicting Blind Geothermal Systems

Convective geothermal systems with no recent surface manifestation (blind systems) are known to occur in active geothermal fields throughout the world. For example, blind systems constitute nearly 40% of known systems in Nevada, and it is likely that far more are yet to be discovered (Faulds and Hinz, 2015). Conceptual models for these inconspicuous geothermal resources vary, but typically an impermeable layer blocks the ascent of fluids, or cold influx of shallow groundwater may dilute or divert a rising plume (Dobson, 2016). It is conceivable that similar blind systems exist in the Canadian Cordillera, masked by high infiltration rates of cold meteoric water. Precipitation rates are higher in the Canadian Cordillera than in the arid Great Basin of the southwestern United States, and thick glacial overburden may facilitate near-surface dispersion and dilution of any ascending plumes of geothermal brine. At least one blind geothermal system has been identified in the Canadian Cordillera, in the Bluebell

mine at Riondel (Figure 3); during mine operation in 1956, workers encountered 20–30°C water flowing from cracks at 90–1000 liters per second (L/sec) at a depth of ~300 m below ground (Desrochers, 1992). This thermal water did not flow to the surface, or, if it did, it had already cooled below detectable levels. It is a statistical likelihood that other blind systems remain undiscovered elsewhere in the Canadian Cordillera, particularly due to the low "degree-of-exploration" (Coolbaugh et al., 2006) in the area. A first-order prediction of their location may come from identifying where local zones of stress concentration may occur (i.e., at favorable structural settings such as fault terminations, intersections or step-overs), given the orientation of faults in the current crustal stress field. A few possible locations in southeastern BC stand out as candidates for blind systems in our structural framework: the right-stepover (releasing bend) at the northernmost end of the Columbia River fault near the Mica Dam (Figures 1 and 2), the right-stepover (releasing bend) in Duncan Lake (Figure 1 and 3), and the intersection of the Beaver River, RMT, and Chancellor faults, at the south end of Kinbasket Lake (Figure 1 and 3). However, these predictions are speculative and further investigation is required.

5.6 Broader Tectonic Relationships

The North American Cordillera, from California in the south to Alaska in the north, has been subject to widespread dextral shear, both diffuse and discrete, from the Jurassic to present. Geological evidence points to large dextral displacements on several major faults throughout the late Mesozoic and Cenozoic, while geophysical and geodetic surveys reveal modern dextral strain across broad regions of western North America. In our study region in southeastern BC, Eocene extension is commonly thought to be the most recent phase of tectonism (Clague, 1974; Lane, 1984; Parrish et al., 1988; van der Velden and Cook, 1996; Fraser et al., 2021), but the data presented in this paper show that dextral shear is more recent in this region, consistent with the broader neotectonic setting and regional trends in seismicity. The most prominent dextral structure in the Canadian Cordillera is the Northern Rocky Mountain Trench – Tintina Trench fault system (Figure 1). In the Yukon, Cretaceous geological units are offset by at least 400 km across the Tintina Trench fault zone (Roddick, 1967). Johnston (1999) argued that an additional 400 km of dextral displacement may be accommodated within synkinematic mid Cretaceous intrusions in the northern Cordillera. In northeastern BC, the Northern Rocky Mountain Trench fault and subsidiary parallel structures (Kutcho and Pinchi faults) are collectively thought to have accommodated up to 1000 km of displacement through the Cretaceous to the Eocene, based on offsets between geological units (Gabrielse, 1985).

Farther south, large dextral displacements are not as easily distinguished. Northeast of Prince George, the Northern Rocky Mountain Trench fault intersects with the SRMT fault, which extends a further ~850 km along the western edge of the Rocky Mountains to northwestern Montana. No significant dextral offsets have been observed along the SRMT fault, despite the fact that its strike deviates only 20°

counterclockwise from the Northern Rocky Mountain Trench fault. McMechan (2000) showed that dextral displacement of ~60 km occurs in the Walker Creek fault zone near the intersection of the northern and southern trench segments and suggested this deformation was late Cretaceous to Eocene in age. Even further south, McDonough and Simony (1989) documented the dextral oblique Valemount Strain Zone, but concluded it was related to the Jurassic(?) Bear Foot thrust. Murphy (1990) documented dextral mylonites at the northern end of Kinbasket Lake along the SRMT and estimated a maximum of 55 km of displacement occurred between 135 and 51 Ma.

Fraser et al. (2021) identified a late-Miocene-to-present phase of extension based on low temperature thermochronological data. They suggest this may be due to orogenic collapse as a result of the high gravitational potential of the Cordillera, a conclusion that seems at odds with the principal stress directions inferred from focal mechanisms and borehole breakouts in the region, which are dominantly compressive (Ristau et al., 2007; Heidbach et al., 2018). We suggest the late Miocene to present extension may instead be a local phenomena related to exhumation at releasing bends in the overall dextral system. Fraser et al. (2021) also note a switch between west-side-down and east-side-down motion across the steeply-dipping SRMT fault, which in our view is more consistent with an overall pattern of strike-slip faulting rather than normal faulting.

Prior to our study, no dextral kinematic indicators or displacements had previously been observed on the SRMT south of the Kinbasket Lake mylonites. Instead, the major faults of southeastern BC are considered by most authors to be part of an array of Eocene normal faults. Any dextral displacement south of ~53°N is thought to be partitioned between several en-echelon fault structures farther to the west. Several authors have argued that the Fraser – Straight Creek fault (Figure 1) accommodates ~100 km of Late Cretaceous to Eocene dextral displacement (Kleinspehn, 1985; Coleman and Parrish, 1991). The Fraser – Straight Creek fault truncates the Yalakom fault at a low angle, which is believed to have accommodated an additional 100 km of dextral slip (Figure 1). Price and Carmichael (1986) fit a small circle to the Northern Rocky Mountain Trench, Tintina Trench, and Fraser – Straight Creek fault systems, concluding that the two structures were mechanically coupled, and that the Fraser – Straight Creek accommodated 100 km of the 450 km displacement on the Northern Rocky Mountain Trench and Tintina faults – the remaining 350 km of displacement being accommodated through oblique convergence in the southern Canadian Rockies. However, most of the shortening accommodated in the southern Canadian Rockies occurred in or before the Late Cretaceous (Pana and Van Der Pluijm, 2015) and mostly predated Eocene dextral slip along the Northern Rocky Mountain Trench. The exception might be the Paleocene McConnell thrust which forms the eastern margin of the Rocky Mountains in southern Alberta and which potentially could have overlapped with initation of slip along the Northern Rocky Mountain - Tintina trench fault.

In the western parts of the Canadian Cordillera, brittle faults have been shown to be active post-Eocene. The Harrison Lake shear zone (Figure 1) and associated structures (which are host to several thermal springs) are believed to have been active in the late Cretaceous through to the early Neogene (Journeay and Csontos, 1989; Journeay and van Ulden, 1998). The West Coast fault (which also hosts several springs), strikes northwest just offshore of Vancouver Island (Figure 1), and is thought to have been active in the late Jurassic to early Eocene (Muller et al., 1981). No neotectonic studies have been conducted on the West Coast fault, but it is likely to be active today given its position in the outer forearc of an active convergent margin. Along the axis of the Coast Belt (where numerous springs occur), the Coast Shear Zone (Figure 1) exhibits a complex history of motion, including dextral shear, between 65-55 Ma (Klepeis et al., 1998; Rusmore et al., 2001). In the Alaska Panhandle, the Chatham Straight and Border Ranges faults (Figure 1) show evidence for significant dextral shear (150 km and 700 km respectively) in the late Cretaceous to Eocene (Hudson et al., 1982; Smart et al., 1996). South of the BC-Yukon border, the Chatham Strait fault and Coast Shear Zone merge with the Denali fault (Figure 1), which is known to be active from the Eocene to present on various segments (Lanphere, 1978; Bemis et al., 2015; Blais-Stevens et al., 2020). Offshore of northern BC, the transpressional Queen Charlotte - Fairweather fault is active in the present day (Rohr et al., 2000; Cassidy et al., 2014).

5.7 Driving Mechanism

Margin-parallel tractions on the Pacific-North America plate boundary affect the permanent inelastic crustal strain far into the hinterland of the Cordillera, possibly acting as the driving mechanism for current dextral faulting in southeastern BC. In the northern Cordillera, strain from the collision of the Yakutat block is believed to be transferred along a deep crustal decollement manifesting as thrusting in the Mackenzie Mountains (e.g., Leonard et al., 2007). We argue that similar, albeit transpressional, transfer of strain occurs in the southern Cordillera. Stress directions derived from earthquake focal mechanisms are margin-parallel in the Cascadia forearc, and margin-normal in the autochthon to the east of the Canadian Rocky Mountains. Our study area in southeastern BC is in the transition zone between margin-normal and margin-parallel stress, and the dextral faulting we have observed reflects a transition between these two stress domains.

6 CONCLUSIONS

Potential geothermal resources in southeastern BC are likely amagmatic and rely on the deep circulation of thermal fluids along permeable fracture pathways to bring heat close to the surface. Our regional-scale investigation of the structural settings of hydrothermal systems in southeastern BC has revealed a consistent pattern of dextral kinematics on brittle subvertical fault planes coincident with the surface traces of faults previously mapped as Eocene and Jura-Cretaceous in age; dextral kinematic indicators were identified along the Rocky Mountain Trench, Purcell Trench, Columbia River Valley, and

Slocan Valley. The timing of this transpressional deformation is constrained to post-Eocene based on cross-cutting relationships observed in Eocene rocks. The NE-SW maximum stress axis required for these kinematics is consistent with the focal mechanisms of several crustal earthquakes that have occurred in the region, suggesting that transpressional strain has developed following the well-documented period of crustal extension in the Eocene. This NE-SW stress field in southeastern BC likely reflects a transition from the margin-parallel (NNW-SSE) maximum stress orientations within the Cascadia forearc to the orogen-normal (ENE-WSW) maximum stress orientations in the Cordilleran foreland. When placed in the context of the current stress field, two main controls on the location of thermal springs become apparent: on a regional scale, there is a positive correlation between seismicity across the entire Cordillera and the locations of thermal springs. On local scales, dextral fault tips, intersections, and interaction zones are shown to be favourable locations for hydrothermal upwelling.

7 ACKNOWLEDGEMENTS

This research was conducted as part of the University of Alberta's Future Energy Systems project: Imaging, Characterizing, and Modelling Canada's Geothermal Resources, a research initiative funded by the Canada First Research Excellence Fund. Additional support came from a Canada Graduate Scholarship – Master's Program award from the Natural Sciences and Engineering Research Council, a Hugh C. Morris Fellowship from the Kimberley Foundation, and a graduate student scholarship from Geoscience BC. Noah Van Camp and Sam Johnson are owed tremendous thanks for their efforts as field assistants. James Faulds and Erin Beutel are thanked for their thorough, constructive reviews that substantially improved the manuscript.

8 REFERENCES CITED

Adams, J., Allen, T., Halchuk, S., and Kolaj, M., 2019, Canada's 6th Generation Seismic Hazard Model, as Prepared for the 2020 National Building Code of Canada, *in* Proceedings 17th World Conference on Earthquake Engineering, Quebec City.

Agemar, T., Weber, J., and Schulz, R., 2014, Deep Geothermal Energy Production in Germany: Energies, v. 7, p. 4397–4416, doi:10.3390/en7074397.

Allen, D.M., Grasby, S.E., and Voormeij, D.A., 2006, Determining the circulation depth of thermal springs in the southern Rocky Mountain Trench, south-eastern British Columbia, Canada using geothermometry and borehole temperature logs: Hydrogeology Journal, v. 14, p. 159–172, doi:10.1007/s10040-004-0428-z.

American Geological Institute, 2003, Global GIS: volcanoes of the world:, https://earthworks.stanford.edu/catalog/harvard-glb-volc (accessed July 2019).

Anderson, E.M., 1905, The dynamics of faulting: Transactions of the Edinburgh Geological Society, v. 8, p. 387–402, doi:10.1144/transed.8.3.387.

873 Angelier, J., 1984, Tectonic analysis of fault slip data sets: Journal of Geophysical Research: Solid Earth,
874 v. 89, p. 5835–5848, doi:10.1029/JB089iB07p05835.

875 Archibald, D.A., Glover, J.K., Price, R.A., Farrar, E., and Carmichael, D.M., 1983, Geochronology and
876 tectonic implications of magmatism and metamorphism, southern Kootenay Arc and
877 neighbouring regions, southeastern British Columbia. Part I: Jurassic to mid-Cretaceous:
878 Canadian Journal of Earth Sciences, v. 20, p. 1891–1913, doi:10.1139/e84-062.

879 Balfour, N.J., Cassidy, J.F., Dosso, S.E., and Mazzotti, S., 2011, Mapping crustal stress and strain in
880 southwest British Columbia: Journal of Geophysical Research, v. 116, p. 1–11,
881 doi:10.1029/2010JB008003.

882 Barton, C.A., Zoback, M.D., and Moos, D., 1995, Fluid flow along potentially active faults in crystalline
883 rock: Geology, v. 23, p. 683–686, doi:10.1130/0091-7613(1995)023<0683:FFAPAF>2.3.CO.

884 Bemis, S.P., Weldon, R.J., and Carver, G.A., 2015, Slip partitioning along a continuously curved fault:
885 Quaternary geologic controls on Denali fault system slip partitioning, growth of the Alaska
886 Range, and the tectonics of south-central Alaska: Lithosphere, v. 7, p. 235–246,
887 doi:10.1130/L352.1.

888 Blackwell, D.D., and Richards, M., 2004, Geothermal Map of North America: AAPG Map,
889 https://www.smu.edu/Dedman/Academics/Departments/EarthSciences/Research/GeothermalLab/
890 DataMaps/GeothermalMapofNorthAmerica (accessed July 2019).

891 Blais-Stevens, A., Clague, J.J., Brahney, J., Lipovsky, P., Haeussler, P.J., and Menounos, B., 2020,
892 Evidence for Large Holocene Earthquakes along the Denali Fault in Southwest Yukon, Canada:
893 Environmental and Engineering Geoscience, v. 26, p. 149–166, doi:10.2113/EEG-2263.

894 Brown, D.A., Doughty, T.P., and Stinson, P., 1994, Preliminary Geology of the Creston Map Area,
895 Southeastern British Columbia (82F/2): BC Geological Survey Geological Fieldwork 1994 Paper
896 1995-1, 135–155 p.

897 Brown, D.A., and MacLeod, R.I., 2011, Geology, Boswell, British Columbia: Geological Survey of
898 Canada Open File 6310.

899 Caine, J.S., Evans, J.P., and Forster, C.B., 1996, Fault zone architecture and permeability structure:
900 Geology, v. 24, p. 1025–1028, doi:10.1130/0091-7613(1996)024<1025.

901 Canadian Geochronology Knowledgebase, 2013, https://www.nrcan.gc.ca/earth-sciences/geography/atlas-
902 canada/canadian-geochronology-knowledgebase/18211#reccit.

903 Caron, M., Grasby, S.E., and Ryan, M.C., 2007, Spring geochemistry: a tool for mineral exploration in
904 the south Nahanni River basin of the Mackenzie Mountains, Northwest Territories: Geological
905 Survey of Canada Open File 5344, 31–74 p.

906 Carr, S.D., 1992, Tectonic setting and U-Pb geochronology of the Early Tertiary Ladybird Leucogranite
907 Suite, Thor-Odin - Pinnacles Area, Southern Omineca Belt, British Columbia: Tectonics, v. 11, p.
908 258–278, doi:10.1029/91TC01644.

909 Carr, S., 1986, The Valkyr Shear Zone and the Slocan Lake Fault: Eocene structures that bound the
910 Valhalla Complex, southeastern British Columbia, doi:10.3102/00346543067001043.

Carr, S.D., Parrish, R.R., and Brown, R.L., 1987, Eocene structural development of the Valhalla Complex, southeastern British Columbia: Tectonics, v. 6, p. 175–196, doi:10.1029/TC006i002p00175.

Cassidy, J.F., Rogers, G.C., and Hyndman, R.D., 2014, An Overview of the 28 October 2012 Mw 7.7 Earthquake in Haida Gwaii, Canada: A Tsunamigenic Thrust Event Along a Predominantly Strike-Slip Margin: Pure and Applied Geophysics, v. 171, p. 3457–3465, doi:10.1007/s00024-014-0775-1.

Célérier, B., Etchecopar, A., Bergerat, F., Vergely, P., Arthaud, F., and Laurent, P., 2012, Inferring stress from faulting: From early concepts to inverse methods: Tectonophysics, v. 581, p. 206–219, doi:10.1016/j.tecto.2012.02.009.

Chamberlain, V.E., Lambert, R.S.J., and Holland, J.G., 1985, Geochemistry and geochronology of the gneisses east of the Southern Rocky Mountain Trench, near Valemount, British Columbia: Canadian Journal of Earth Sciences, v. 22, p. 980–991, doi:10.1139/e85-103.

Charlesworth, H.A.K., 1959, Some suggestions on the structural development of the Rocky Mountains of Canada: Journal of the Alberta Society of Petroleum Geologists, v. 7.

Clague, J.J., 1974, The St. Eugene Formation and the Development of the Southern Rocky Mountain Trench: Canadian Journal of Earth Sciences, v. 11, p. 916–938, doi:10.1139/e74-091.

Coleman, M.E., and Parrish, R.R., 1991, Eocene dextral strike-slip and extensional faulting in the Bridge River Terrane, southwest British Columbia: Tectonics, v. 10, p. 1222–1238, doi:10.1029/91TC01078.

Cook, F. a, Varsek, J.L., Clowes, R.M., Kanasewich, E.R., Spencer, C.S., Parrish, R.R., Brown, R.L., Carr, S.D., and Johnson, B.J., 1992, LITHOPROBE crustal reflection cross section of the southern Canadian Cordillera, 1, Foreland thrust and fold belt to Fraser River Fault: Tectonics, v. 11, p. 12–35.

Coolbaugh, M.F., Raines, G.L., Zehner, R.S.E., Shevenell, L., and Williams, C.F., 2006, Prediction and discovery of new geothermal resources in the Great Basin: Multiple evidence of a large undiscovered resource base, *in* GRC Transactions, v. 30.

Corbett, C.R., and Simony, P.S., 1984, The Champion Lake Fault in the Trail-Castlegar Area of Southeastern British Columbia, *in* Geological Survey of Canada Current Research, Paper 84-1A, p. 103–104.

Craig, J.W., Faulds, J.E., Hinz, N.H., Earney, T.E., Schermerhorn, W.D., Siler, D.L., Glen, J.M., Peacock, J., Coolbaugh, M.F., and Deoreo, S.B., 2021, Discovery and analysis of a blind geothermal system in southeastern Gabbs Valley, western Nevada, USA: Geothermics, v. 97, doi:10.1016/j.geothermics.2021.102177.Cui, Y., Miller, D., Schiarizza, P., and Diakow, L.J., 2017, British Columbia Digital Geology: British Columbia Geological Survey Open File 2017-8, http://cmscontent.nrs.gov.bc.ca/geoscience/PublicationCatalogue/OpenFile/BCGS_OF2017-08.pdf (accessed July 2019).

Curewitz, D., and Karson, J.A., 1997, Structural settings of hydrothermal outflow: Fracture permeability maintained by fault propagation and interaction: Journal of Volcanology and Geothermal Research, v. 79, p. 149–168, doi:10.1016/S0377-0273(97)00027-9.

951 Desrochers, D.T., 1992, Geothermal feasibility study for the use of hot water near Riondel, British
952 Columbia: Geological Survey of Canada Open File 2502.

953 Doblas, M., 1998, Slickenside kinematic indicators: Tectonophysics, v. 295, p. 187–197,
954 doi:10.1016/S0040-1951(98)00120-6.

955 Dobson, P.F., 2016, A Review of Exploration Methods for Discovering Hidden Geothermal Systems, *in*
956 GRC Transactions, v. 40, p. 695–706.

957 Doughty, P.T., and Price, R.A., 2000, Geology of the Purcell Trench rift valley and Sandpoint
958 Conglomerate: Eocene en echelon normal faulting and synrift sedimentation along the eastern
959 flank of the Priest River metamorphic complex, northern Idaho: GSA Bulletin, v. 112, p. 1356–
960 1374.

961 Doughty, P.T., and Price, R.A., 1999, Tectonic evolution of the Priest River complex, northern Idaho and
962 Washington: A reappraisal of the Newport fault with new insights on metamorphic core complex
963 formation: Tectonics, v. 18, p. 375–393, doi:10.1029/1998TC900029.

964 Dresen, G., 1991, Stress distribution and the orientation of Riedel shears: Tectonophysics, v. 188, p. 239–
965 247, doi:10.1016/0040-1951(91)90458-5.

966 Farquharson, N., Schubert, A., and Steiner, U., 2016, Geothermal Energy in Munich (and Beyond): A
967 Geothermal City Case Study, *in* GRC Transactions, v. 40, p. 189–196.

968 Faulds, J., and Hinz, N., 2015, Favorable Tectonic and Structural Settings of Geothermal Systems in the
969 Great Basin Region, Western USA: Proxies for Discovering Blind Geothermal Systems:
970 Proceedings World Geothermal Congress, p. 6.

971 Faulds, J.E., Hinz, N., Kreemer, C., and Coolbaugh, M., 2012, Regional Patterns of Geothermal Activity
972 in the Great Basin Region, Western USA: Correlation With Strain Rates: GRC Transactions, v.
973 36, p. 6.

974 Ferguson, G., and Grasby, S.E., 2011, Thermal springs and heat flow in North America: Geofluids, v. 11,
975 p. 294–301, doi:10.1111/j.1468-8123.2011.00339.x.

976 Finley, T., Prush, V., Nissen, E., Miller, B., Sethanant, I., Cassidy, J., and Rowe, C., 2021, Preliminary
977 Evidence of Late Quaternary Faulting in the Rocky Mountain Trench from New Lidar Data and
978 Field Investigations, *in* American Geophysical Union Fall Meeting, New Orleans.

979 Foo, W.K., 1979, Evolution of Transverse Structures Linking the Purcell Anticlinorium to the Western
980 Rocky Mountains Near Canal Flats, British Columbia: Queens University.

981 Fossen, H., and Cavalcante, G.C.G., 2017, Shear zones – A review: Earth-Science Reviews, v. 171, p.
982 434–455, doi:10.1016/j.earscirev.2017.05.002.

983 Fraser, K.I., Enkelmann, E., Jess, S., Gilbert, H., and Grieco, R., 2021, Resolving the Cenozoic History of
984 Rock Exhumation Along the Central Rocky Mountain Trench Using Apatite Low-Temperature
985 Thermochronology: Tectonics, v. 40, p. e2021TC006847, doi:10.1029/2021TC006847.

Frohlich, C., 1992, Triangle diagrams: ternary graphs to display similarity and diversity of earthquake focal mechanisms: Physics of the Earth and Planetary Interiors, v. 75, p. 193–198, doi:10.1016/0031-9201(92)90130-N.

Gabrielse, H., 1985, Major dextral transcurrent displacements along the Northern Rocky Mountain Trench and related lineaments in north-central British Columbia: Bulletin of the Geological Society of America, v. 96, p. 1–14, doi:10.1130/0016-7606(1985)96<1:MDTDAT>2.0.CO;2.

Gabrielse, H., and Yorath, C.J., 1991, Tectonic Synthesis, *in* Geology of the Cordilleran orogen in Canada, Geological Survey of Canada, v. 4, p. 680–705.

Gal, L.P., and Ghent, E.D., 1990, Metamorphism in the Solitude Range, southwestern Rocky Mountains, British Columbia: comparison with adjacent Omineca Belt rocks and tectonometamorphic implications for the Purcell Thrust: Canadian Journal of Earth Sciences, v. 27, p. 1511–1520.

Grasby, S.E. et al., 2012, Geothermal Energy Resource Potential of Canada: Geological Survey of Canada Open File 6914, 322 p.

Grasby, S.E., Ferguson, G., Bartier, P., and Neville, L., 2019, Seismic induced flow disruption of Gandll K'in Gwaay.yaay thermal springs, Gwaii Haanas National Park Reserve, Canada: Applied Geochemistry, v. 103, p. 118–130, doi:10.1016/j.apgeochem.2019.03.005.

Grasby, S.E., and Hutcheon, I., 2001, Controls on the distribution of thermal springs in the southern Canadian Cordillera: Canadian Journal of Earth Sciences, v. 38, p. 427–440, doi:10.1139/e00-091.

Heidbach, O. et al., 2018, The World Stress Map database release 2016: Crustal stress pattern across scales: Tectonophysics, v. 744, p. 484–498, doi:10.1016/j.tecto.2018.07.007.

Henderson, G.G.L., 1954, Geology of the Stanford Range of the Rocky Mountains: British Columbia Department of Mines Bulletin, v. 35, p. 93.

Höy, T., 1993, Geology of the Purcell Supergroup in the Fernie west-half map area, southeastern British Columbia: Victoria, B.C., British Columbia, Ministry of Energy, Mines and Petroleum Resources.

Hudson, T., Plafker, G., and Dixon, K., 1982, Horizontal offset history of the Chatham Strait fault: U.S. Geological Survey Circular 844, 5 p.

Hyndman, D.W., 1968, Petrology and structure of Nakusp map area, British Columbia: Bulletin 161, doi:10.4095/102320.

Hyndman, R.D., and Lewis, T.J., 1995, Review: The thermal regime along the southern Canadian Cordillera Lithoprobe corridor: Canadian Journal of Earth Sciences, v. 32, p. 1611–1617, doi:10.1139/e95-129.

Jess, S., Enkelmann, E., Grasby, S.E., and Fraser, K., 2021, Determining the Lifespan of Hydrothermal Systems Using Thermochronology and Thermal Modeling: Journal of Geophysical Research: Earth Surface, v. 126, p. e2021JF006286, doi:10.1029/2021JF006286.

1022 Johnston, S.T., 1999, Large-scale coast-parallel displacements in the Cordillera: a granitic resolution to a
1023 paleomagnetic dilemma: Journal of Structural Geology, v. 21, p. 1103–1108, doi:10.1016/S0191-
1024 8141(99)00015-2.

1025 Journeay, J.M., and Csontos, L., 1989, Preliminary Report On the Structural Setting Along the Southeast
1026 Flank of the Coast Belt, British Columbia: 89–1E, 89–1E p., doi:10.4095/127480.

1027 Journeay, J.M., and van Ulden, J., 1998, Neogene structural elements of northern Cascadia, British
1028 Columbia: 1998-A/B, 1998-A/B p., doi:10.4095/209503.

1029 Kao, H., Shan, S.-J., Bent, A., Woodgold, C., Rogers, G., Cassidy, J.F., and Ristau, J., 2012, Regional
1030 Centroid-Moment-Tensor Analysis for Earthquakes in Canada and Adjacent Regions: An Update:
1031 Seismological Research Letters, v. 83, p. 505–515, doi:10.1785/gssrl.83.3.505.

1032 Kimball, S., 2010, Favourability Map of British Columbia Geothermal Resources: The University of
1033 British Columbia,
1034 http://pics.uvic.ca/sites/default/files/uploads/publications/kimball_thesis_2010.pdf.

1035 Kleinspehn, K.L., 1985, Cretaceous sedimentation and tectonics, Tyaughton–Methow Basin,
1036 southwestern British Columbia: Canadian Journal of Earth Sciences, v. 22, p. 154–174,
1037 doi:10.1139/e85-014.

1038 Klepeis, K.A., Crawford, M.L., and Gehrels, G., 1998, Structural history of the crustal-scale Coast shear
1039 zone north of Portland Canal, southeast Alaska and British Columbia: Journal of Structural
1040 Geology, v. 20, p. 883–904, doi:10.1016/S0191-8141(98)00020-0.

1041 Kraft, J.L., 2013, Stratigraphy, paleogeography and tectonic evolution of early Paleozoic to Triassic
1042 pericratonic strata in the northern Kootenay Arc, southeastern Canadian Cordillera, British
1043 Columbia: ERA, doi:10.7939/R3KD89.

1044 Kraft, J.L., Thompson, R.I., and Dhesi, P., 2011, Geology, Beaton, British Columbia: Geological Survey
1045 of Canada Open File 6574.

1046 Kreemer, C., Blewitt, G., and Klein, E.C., 2014, A geodetic plate motion and Global Strain Rate Model:
1047 Geochemistry, Geophysics, Geosystems, v. 15, p. 3849–3889, doi:10.1002/2014GC005407.

1048 Kubli, T.E., and Simony, P.S., 1994, The Dogtooth duplex, a model for the structural development of the
1049 northern Purcell Mountains: Canadian Journal of Earth Sciences, v. 31, p. 1672–1686.

1050 Lane, L.S., 1984, Brittle deformation in the Columbia River fault zone near Revelstoke, southeastern
1051 British Columbia: Canadian Journal of Earth Sciences, v. 21, p. 584–598, doi:10.1139/e84-063.

1052 Lanphere, M.A., 1978, Displacement history of the Denali fault system, Alaska and Canada: Canadian
1053 Journal of Earth Sciences, v. 15, p. 817–822, doi:10.1139/e78-086.

1054 Lemieux, Y., Thompson, R.I., and Erdmer, P., 2003, Stratigraphy and structure of the Upper Arrow Lake
1055 area, southeastern British Columbia: new perspectives for the Columbia River Fault Zone:
1056 Geological Survey of Canada Current Research 2003-A7.

Leonard, L.J., Hyndman, R.D., Mazzotti, S., Nykolaishen, L., Schmidt, M., and Hippchen, S., 2007, Current deformation in the northern Canadian Cordillera inferred from GPS measurements: Journal of Geophysical Research: Solid Earth, v. 112, p. 1–15, doi:10.1029/2007JB005061.

Majorowicz, J., and Grasby, S.E., 2010, Heat flow, depth–temperature variations and stored thermal energy for enhanced geothermal systems in Canada: Journal of Geophysics and Engineering, v. 7, p. 232–241, doi:10.1088/1742-2132/7/3/002.

Mazzotti, S., Leonard, L.J., Cassidy, J.F., Rogers, G.C., and Halchuk, S., 2011, Seismic hazard in western Canada from GPS strain rates versus earthquake catalog: Journal of Geophysical Research: Solid Earth, v. 116, p. 1–17, doi:10.1029/2011JB008213.

McClymont, A., Ernst, E., Bauman, P., and Payne, N., 2016, Integrating Geophysical and Geotechnical Engineering Methods for Assessment of Pipeline Geohazards, *in* Volume 3: Operations, Monitoring and Maintenance; Materials and Joining, Calgary, Alberta, Canada, American Society of Mechanical Engineers, doi:10.1115/IPC2016-64222.

McDonough, M.R., and Morrison, M.L., 1990, Ptarmigan Creek West Half, British Columbia (83D/10): Geological Survey of Canada Open File 2305.

McDonough, M.R., and Simony, P.S., 1988, Structural evolution of basement gneisses and Hadrynian cover, Bulldog Creek area, Rocky Mountains, British Columbia: Canadian Journal of Earth Sciences, v. 25, p. 1687–1702, doi:10.1139/e88-159.

McDonough, M.R., and Simony, P.S., 1989, Valemount strain zone: a dextral oblique-slip thrust system linking the Rocky Mountain and Omineca belts of the southeastern Canadian Cordillera: Geology, v. 17, p. 237–240, doi:10.1130/0091-7613(1989)017<0237:VSZADO>2.3.CO;2.

McKenzie, D.P., 1969, The relation between fault plane solutions for earthquakes and the directions of the principal stresses: Bulletin of the Seismological Society of America, v. 59, p. 591–601.

McMechan, M.E., 2000, Walker Creek fault zone, central Rocky Mountains, British Columbia-southern continuation of the Northern Rocky Mountain Trench fault zone: Canadian Journal of Earth Sciences, v. 37, p. 1259–1273, doi:10.1139/e00-038.

Meixner, J., Schill, E., Grimmer, J.C., Gaucher, E., Kohl, T., and Klingler, P., 2016, Structural control of geothermal reservoirs in extensional tectonic settings: An example from the Upper Rhine Graben: Journal of Structural Geology, v. 82, p. 1–15, doi:10.1016/j.jsg.2015.11.003.

Menzies, C.D., Teagle, D.A.H., Niedermann, S., Cox, S.C., Craw, D., Zimmer, M., Cooper, M.J., and Erzinger, J., 2016, The fluid budget of a continental plate boundary fault: Quantification from the Alpine Fault, New Zealand: Earth and Planetary Science Letters, v. 445, p. 125–135, doi:10.1016/j.epsl.2016.03.046.

Moynihan, D., and Pattison, D.R.M., 2008, Origin of the Kootenay Lake Metamorphic High , Southeastern British Columbia: British Columbia Geological Survey Geological Fieldwork 2008–1, 147–158 p.

Muller, J.E., Cameron, B.E.B., and Northcote, K.E., 1981, Geology and mineral deposits of the Nootka Sound map-area (92E) Vancouver Island, British Columbia.: Geological Survey of Canada Paper 80-16, 59 p.

Murphy, D.C., 1990, Direct evidence for dextral strike-slip displacement from mylonites in the southern Rocky Mountain Trench near Valemount, British Columbia: Geological Survey of Canada Current Research, Paper 90-1E.

North, F.K., and Henderson, G.G.L., 1954a, Summary of the Geology of the Southern Rocky Mountains of Canada: Guide Book Fourth Annual Field Conference Banff-Golden-Radium, p. 15–81.

North, F.K., and Henderson, G.G.L., 1954b, The Rocky Mountain Trench: Canadian Society of Petroleum Geologists,.

Pana, D., and Van Der Pluijm, B., 2015, Orogenic pulses in the Alberta Rocky Mountains: Radiometric dating of major faults and comparison with the regional tectono-stratigraphic record | GSA Bulletin | GeoScienceWorld: GSA Bulletin, v. 127, p. 480–502.

Parrish, R.R., 1981, Geology of the Nemo Lakes belt, northern Valhalla Range, southeast British Columbia: Canadian Journal of Earth Sciences, v. 18, p. 944–958, doi:10.1139/e81-091.

Parrish, R.R., Carr, S.D., and Parkinson, D.L., 1988, Eocene extensional tectonics and geochronology of the Southern Omineca Belt, British Columbia and Washington: Tectonics, v. 7, p. 181–212, doi:10.1029/TC007i002p00181.

Parrish, R.R., and Wheeler, J.O., 1983, A U–Pb zircon age from the Kuskanax batholith, southeastern British Columbia: Canadian Journal of Earth Sciences, v. 20, p. 1751–1756, doi:10.1139/e83-165.

Petit, J.P., 1987, Criteria for the sense of movement on fault surfaces in brittle rocks: Journal of Structural Geology, v. 9, p. 597–608, doi:10.1016/0191-8141(87)90145-3.

Pope, M.C., and Sears, J.W., 1997, Cassiar platform, north-central British Columbia: A miogeoclinal fragment from Idaho: Geology, v. 25, p. 515–518.

Poulton, T.P., and Simony, P.S., 1980, Stratigraphy, sedimentology, and regional correlation of the Horsethief Creek Group (Hadrynian, Late Precambrian) in the northern Purcell and Selkirk Mountains, British Columbia: Canadian Journal of Earth Sciences, v. 17, p. 1708–1724, doi:10.1139/e80-179.

Price, R.A., and Carmichael, D.M., 1986, Geometric test for Late Cretaceous-Paleogene intracontinental transform faulting in the Canadian Cordillera: Geology, v. 14, p. 468–471, doi:10.1130/0091-7613(1986)14<468:GTFLCI>2.0.CO;2.

Purba, J.C.S., Gilbert, H., and Dettmer, J., 2021, Structure and Dynamics of the Southern Rocky Mountain Trench near Valemount, British Columbia, Inferred from Local Seismicity: , p. 13.

Read, P., 1990, Mount Meager Complex, Garibaldi Belt, Southwestern British Columbia: Geoscience Canada, v. 17, p. 167–170.

Read, B., and Brown, R.L., 1981, Columbia River fault zone: southeastern margin of the Shuswap and Monashee complexes, southern British Columbia: v. 1145, p. 1127–1145.

Reyes, A.G., 2015, Low-temperature geothermal reserves in New Zealand: Geothermics, v. 56, p. 138–161, doi:10.1016/j.geothermics.2015.04.004.

1132 Ristau, J., Rogers, G.C., and Cassidy, J.F., 2007, Stress in western Canada from regional moment tensor
1133 analysis: Canadian Journal of Earth Sciences, v. 44, p. 127–148, doi:10.1139/e06-057.

1134 Roddick, J.A., 1967, Tintina Trench: Journal of Geology, v. 75, p. 23–33.

1135 Rogers, G., Cassidy, J., and Ellis, R., 1990, The Prince George, British Columbia, Earthquake of 21
1136 March 1986: Bulletin of the Seismological Society of America, v. 80, p. 1144–1161.

1137 Rogers, G.C., and Ellis, R.M., 1979, The eastern British Columbia earthquake of February 4, 1918:
1138 Canadian Journal of Earth Sciences, v. 16, p. 1484–1493, doi:10.1139/e79-131.

1139 Rogers, G.C., Ellis, R.M., and Hasegawa, H.S., 1980, The McNaughton Lake Earthquake of May 14,
1140 1978: Bulletin of the Seismological Society of America, v. 70, p. 1771–1786.

1141 Rohr, K.M.M., Scheidhauer, M., and Trehu, A.M., 2000, Transpression between two warm mafic plates:
1142 The Queen Charlotte Fault revisited: Journal of Geophysical Research: Solid Earth, v. 105, p.
1143 8147–8172, doi:10.1029/1999JB900403.

1144 Ross, J.V., and Kellerhals, P., 1968, Evolution of the Slocan Syncline in south-central British Columbia:
1145 Canadian Journal of Earth Sciences, v. 5, p. 851–872, doi:10.1139/e68-082.

1146 Rusmore, M.E., Gehrels, G., and Woodsworth, G.J., 2001, Southern continuation of the Coast shear zone
1147 and Paleocene strain partitioning in British Columbia–southeast Alaska: GSA Bulletin, v. 113, p.
1148 961–975, doi:10.1130/0016-7606(2001)113<0961:SCOTCS>2.0.CO;2.

1149 Shipton, Z.K., Soden, A.M., Kirkpatrick, J.D., Bright, A.M., and Lunn, R.J., 2006, How thick is a fault?
1150 Fault displacement-thickness scaling revisited, *in* Abercrombie, R., McGarr, A., Kanamori, H.,
1151 and Di Toro, G. eds., Geophysical Monograph Series, Washington, D. C., American Geophysical
1152 Union, v. 170, p. 193–198, doi:10.1029/170GM19.

1153 Sibson, H., 1996, Structural permeability of fluid-driven fault-fracture meshes: Journal of Structural
1154 Geology, v. 18, p. 1–12, doi:10.1016/0191-8141(96)00032-6.

1155 Siler, D.L., Hinz, N.H., and Faulds, J.E., 2018, Stress concentrations at structural discontinuities in active
1156 fault zones in the western United States: Implications for permeability and fluid flow in
1157 geothermal fields: GSA Bulletin, v. 130, p. 1273–1288, doi:10.1130/B31729.1.

1158 Smart, K.J., Pavlis, T.L., Sisson, V.B., Roeske, S.M., and Snee, L.W., 1996, The Border Ranges fault
1159 system in Glacier Bay National Park, Alaska: evidence for major early Cenozoic dextral strike-
1160 slip motion: Canadian Journal of Earth Sciences, v. 33, p. 1268–1282, doi:10.1139/e96-096.

1161 Stanton, R.J., 1966, The Solution Brecciation Process: GSA Bulletin, v. 77, p. 843–848,
1162 doi:10.1130/0016-7606(1966)77[843:TSBP]2.0.CO;2.

1163 Thompson, R.I., and Dhesi, P., 2009, Geology, Rosebery, British Columbia: Geological Survey of
1164 Canada Open File 6187.

1165 Thompson, R.I., Glombick, P., and Lemieux, Y., 2004a, Geology, Eureka Mountain, British Columbia:
1166 Geological Survey of Canada Open File 4370.

Thompson, R.I., Glombick, P., and Lemieux, Y., 2004b, Geology: Mount Fosthall: Geological Survey of Canada Open File 4377.

Thompson, R.I., Lemieux, Y., Glombick, P., and Dhesi, P., 2009a, Geology, Nakusp, British Columbia: Geological Survey of Canada Open File 6186.

Thompson, R.I., Lemieux, Y., Glombick, P., and Dhesi, P., 2009b, Geology, St. Leon, British Columbia: Geological Survey of Canada Open File 6185.

van der Velden, A.J., and Cook, F.A., 1996, Structure and tectonic development of the southern Rocky Mountain trench: Tectonics, v. 15, p. 517–544, doi:10.1029/95TC03288.

Vollmer, F., 2019, Orient: Spherical Projection and Orientation Data Analysis Software User Manual:, https://www.frederickvollmer.com/orient/download/Orient_User_Manual.pdf (accessed July 2019).

Wessel, P., Luis, J.F., Uieda, L., Scharroo, R., Wobbe, F., Smith, W.H.F., and Tian, D., 2019, The Generic Mapping Tools Version 6: Geochemistry, Geophysics, Geosystems, v. 20, p. 5556–5564, doi:10.1029/2019GC008515.

Woodsworth, G., and Woodsworth, D., 2014, Hot Springs of Western Canada: A Complete Guide: Gordon Soules Book Publishers, 303 p.

Zoback, M.L., 1992, First- and second-order patterns of stress in the lithosphere: The World Stress Map Project: Journal of Geophysical Research: Solid Earth, v. 97, p. 11703–11728, doi:https://doi.org/10.1029/92JB00132.

9 FIGURES

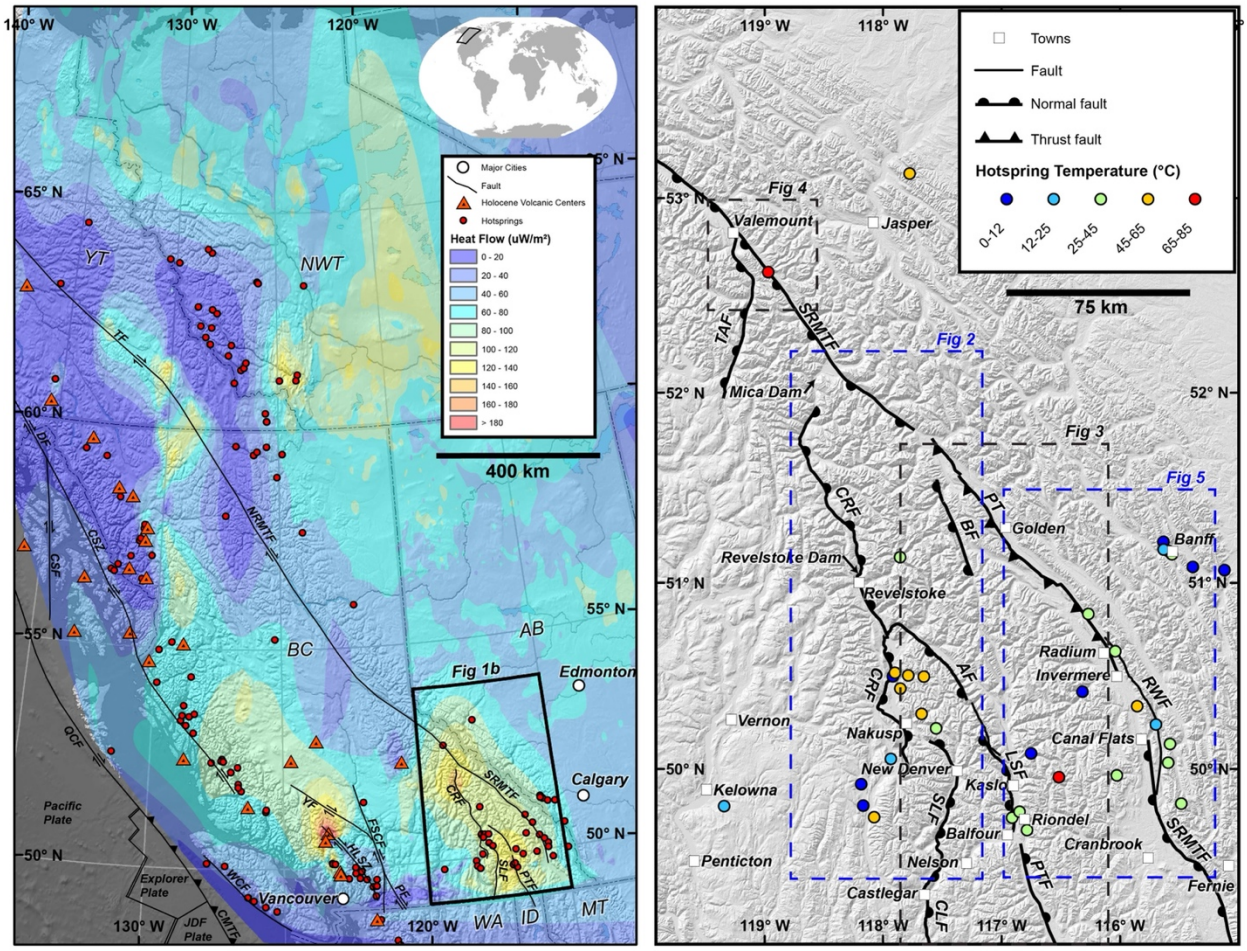

Figure 1. a) Map of the Canadian Cordillera showing heat flow contours (data from Majorowicz and Grasby, 2010), Holocene volcanic centers (American Geological Institute, 2003), thermal springs (Woodsworth and Woodsworth, 2014), and major faults discussed in this paper. The region considered in this study (black rectangle) lies within the Columbia Mountains of southeastern BC, where there is a heat flow anomaly, a cluster of thermal springs, but no volcanic centers. b) Detail of major fault segments in southeastern BC considered in this study and key to subsequent figure locations. Fault abbreviations: AF, Adit fault; BF, Beaver River fault; CLF, Champion Lakes fault; CMTF, Cascadia Megathrust fault; CSF, Chatham Strait fault; CSZ, Coast Shear Zone; CRF, Columbia River fault; DF, Denali fault; FSCF, Fraser-Straight Creek fault; HLSZ, Harrison Lake Shear Zone; LSF, Lakeshore fault; NRMTF, Northern Rocky Mountain Trench fault; PF, Pasayten fault; PT, Purcell Thrust; PTF, Purcell Trench fault; QCF, Queen Charlotte fault; RWF, Redwall fault; SRMTF, Southern Rocky Mountain Trench fault; SLF, Slocan Lake fault; TAF, Thompson Albreda fault; TF, Tintina fault; YF, Yalakom fault.

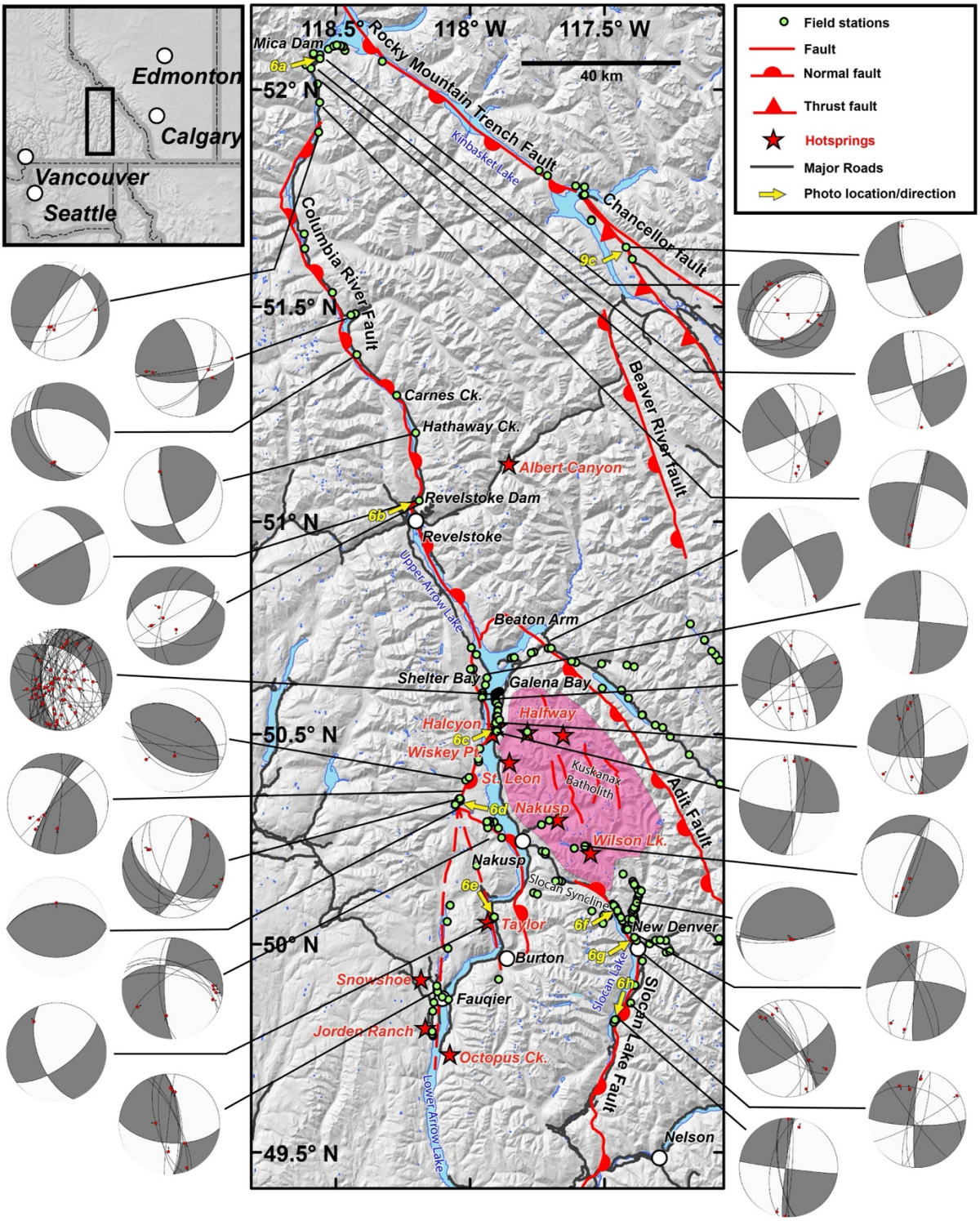

Figure 2. Data collected from the Columbia River and Slocan Lake faults. Lower-hemisphere stereoplots ('beachballs') show fault plane (black great circles) and slickenfibre (red dots) orientations for subsets of data collected as part of this research. P (white) and T (grey) quadrants represent the average kinematics for each subset. Yellow arrows point in direction of photos shown in Figure 6.

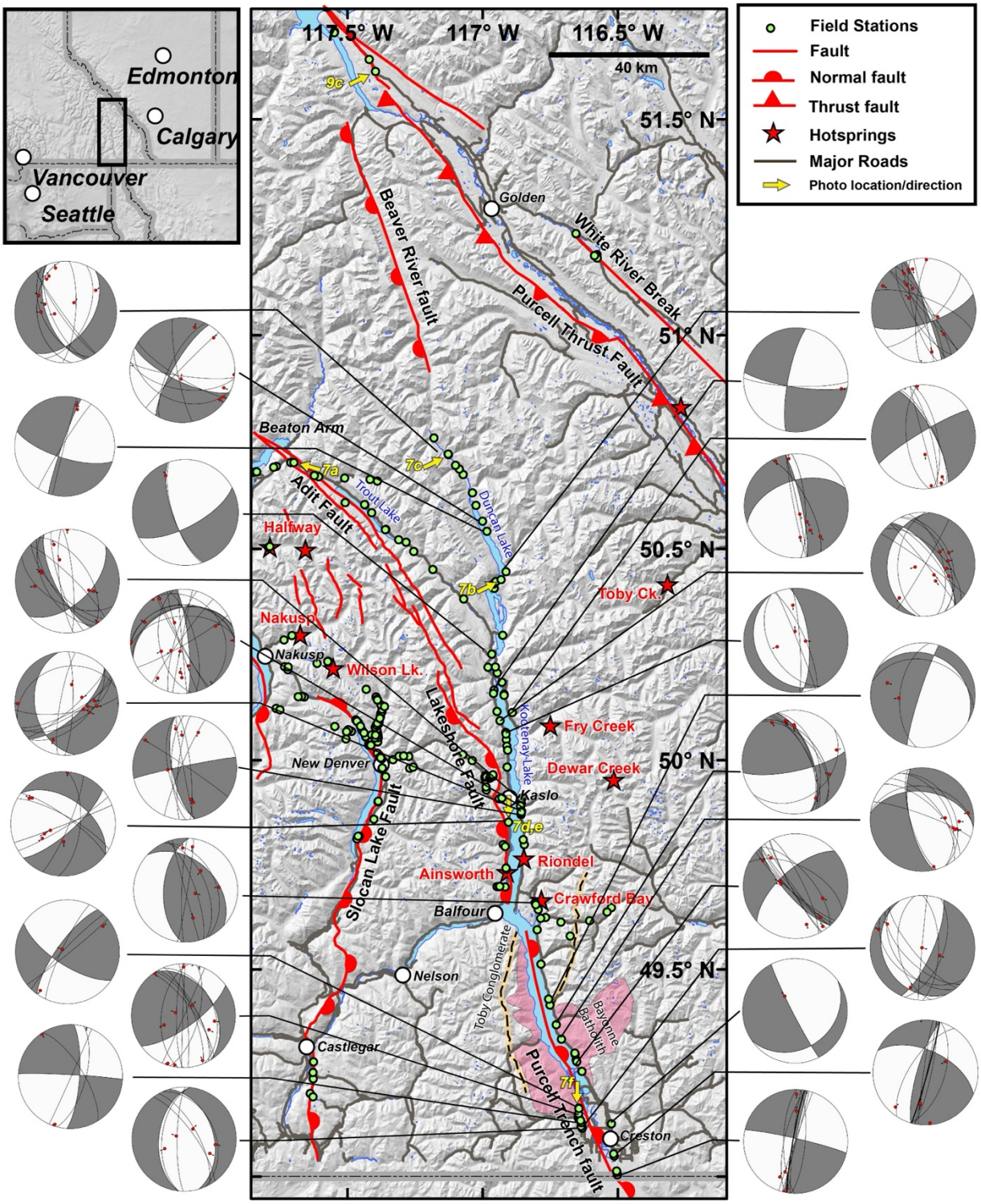

Figure 3. Data collected from the Purcell Trench fault. Lower-hemisphere stereoplots ('beachballs') show fault plane (black great circles) and slickenfibre (red dots) orientations for subsets of data collected as part of this research. P (white) and T (grey) quadrants represent the average kinematics for each subset. Yellow arrows point in direction of photos shown in Figure 7.

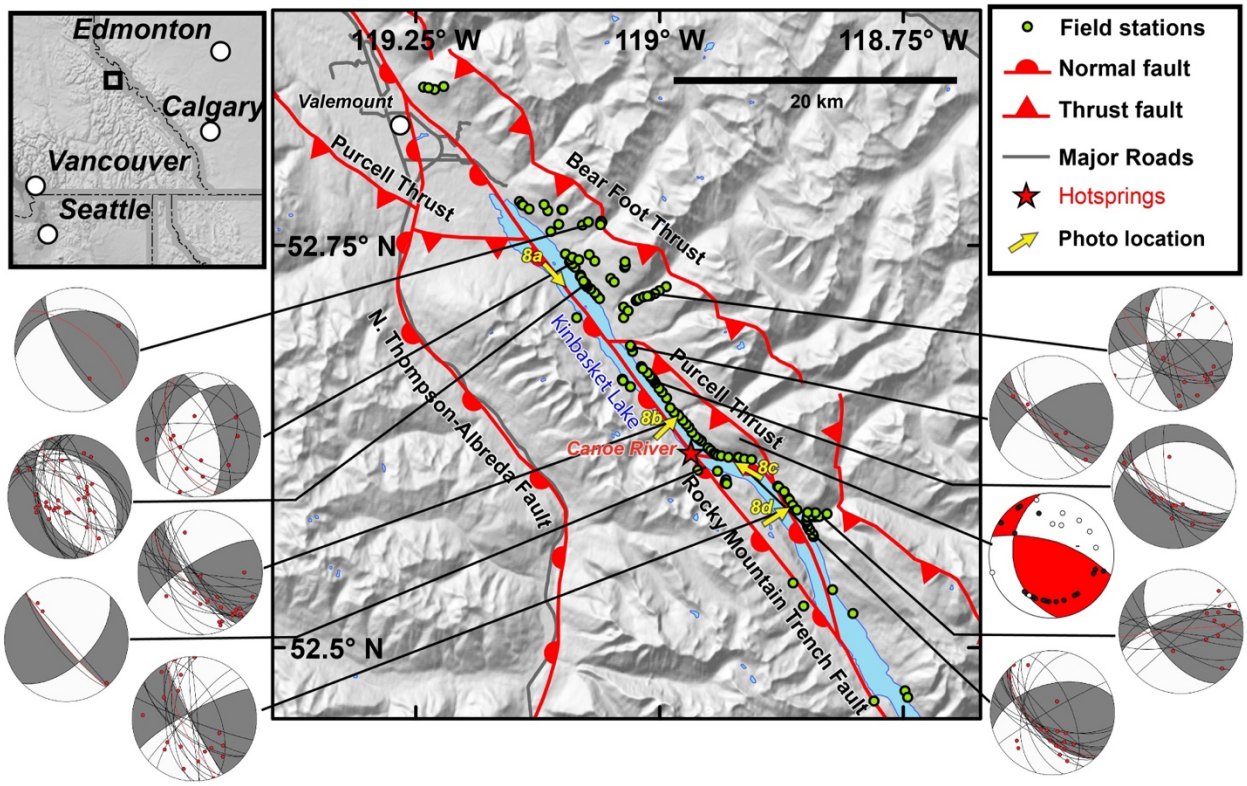

Figure 4. Data collected from the SRMT in the Valemount area. Lower-hemisphere stereoplots ('beachballs') show fault plane (black great circles) and slickenfibres (red dots) orientations for subsets of data collected as part of this research. P (white) and T (grey) quadrants represent the average kinematics for each subset. The red beachball illustrates the kinematics of the 1978 ML 4.8 earthquake (Rogers et al., 1980). Yellow arrows point in direction of photos shown in Figure 8.

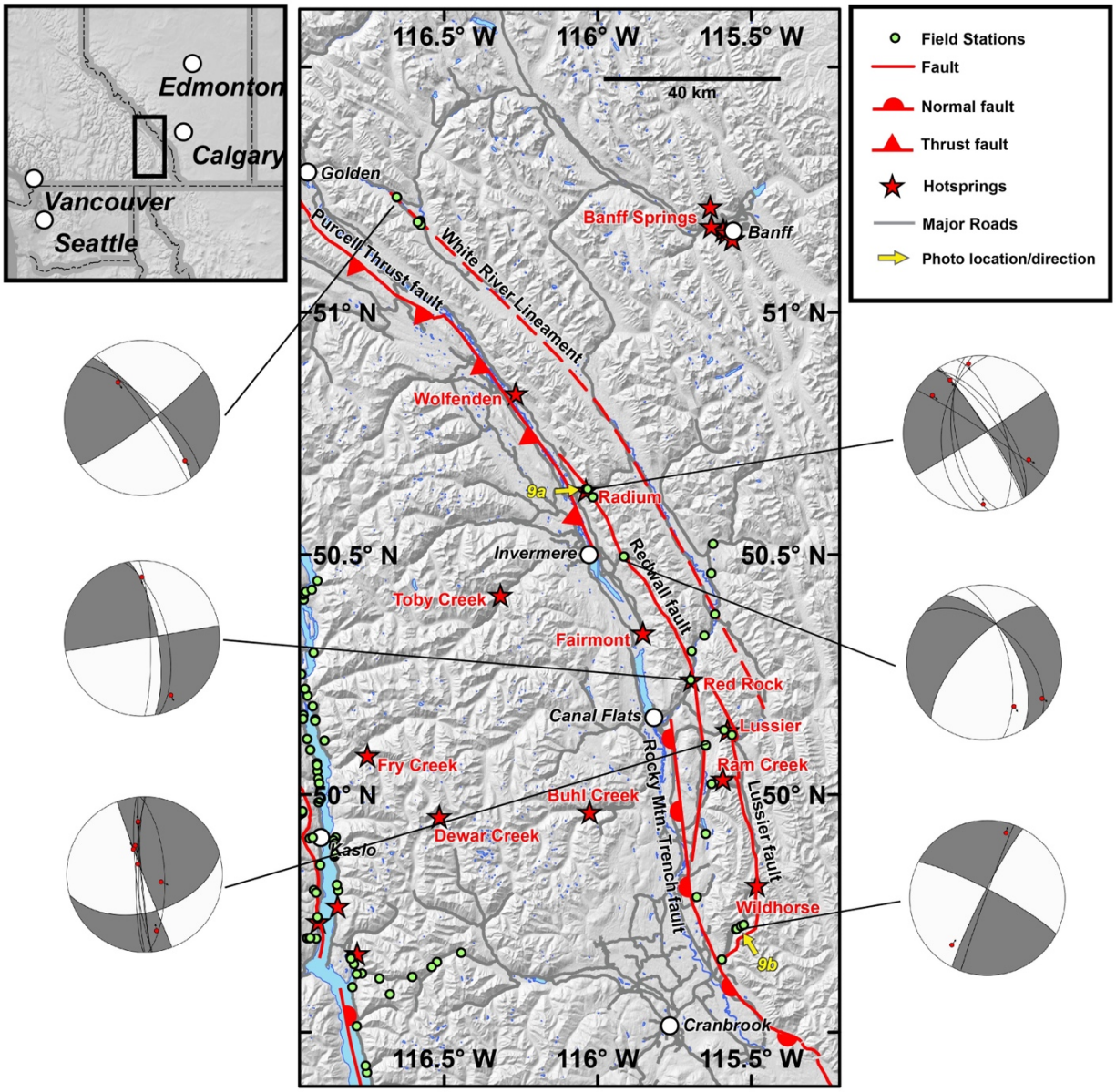

Figure 5. Data collected from the SRMT and Redwall faults. Lower-hemisphere stereoplots ('beachballs') show fault plane (black great circles) and slickenfibre (red dots) orientations for subsets of data collected as part of this research. P (white) and T (grey) quadrants represent the average kinematics for each subset. Yellow arrows point in direction of photos shown in Figure 9.


a)
FP: 235°/41°
SL: 41°–>329°
N
S
b)
FP: 240°/88°
NW
SL: 44°–>248°
SE
c)
FP: 218°/65°
NW
SL: 10°–>221°
SE
d)
S
N
e)
FP: 159°/60°
E
SL: 24°–>324°
W
f)
Tufa
FP: 280°/34°
N
S
g)
N
S
h)
Eocene ductile fabric
Brittle dextral fault
FP: 172°/74°
E
SL: 09°–>195°
W

Figure 6. Photos from the Columbia River and Slocan Lake faults. See Figure 2 for photo locations. Beachballs show kinematics for faults in respective photo. Concentric circles indicate movement out of the page, circles containing an 'x' indicate movement into the page. a) A set of SW-NE striking normal faults (fault: 235°/41°; slickenfibres: 41°→329°) exposed near Mica Dam (lat. 52.0710°N, long. 118.5590°W). Person circled for scale. b) View northeast at outcrop on Highway 23 above the southeastern abutment of the Revelstoke Dam (lat. 51.0486°N, long. 118.1901°W). A splay of the main Columbia River fault exposed here is reinforced with rebar and shotcrete. Dextral slickenfibres (44°→248°) are present on the footwall of the splay fault (240°/88°). c) A 1.2 m gouge zone along Highway 23 near Halcyon Hot Springs (lat. 50.5217°N, long. 117.8998°W). Dextral slickenfibres (10°→221°) characterize the fault (218°/65°). d) Fault mapped as a normal fault (Thompson et al., 2004b), reinterpreted as a reverse fault based on folded footwall and reverse slickenfibres on the hanging wall. This fault occurs in a possible restraining bend of the dextral Columbia River fault (lat. 50.3406°N, long. 118.0394°W). Hammer for scale. e) Subvertical fault plane 159°/60° with dextral slickenfibres (24°→324°) exposed on highway 6, 20km south of Nakusp. f) Broad zone of breccia and gouge striking west (280°/34°) at the north end of Slocan Lake (lat. 50.0983°N, long. 117.4586°W), possibly related to north south shortening in a restraining bend of the Slocan-Columbia River fault system. A tufa deposit occurs where the fault intersects the pre-roadcut ground surface. g) View east at outcrop on Highway 6 north of New Denver (lat. 50.0555°N, long. 117.4323°W). 20 cm wavelength, south-vergent folds deform felsic sills intruded parallel to S1 cleavage (oriented 278°/51°) of the Slocan phyllite. Circle is 1.5 m wide. h) View south at outcrop on Highway 6 south of New Denver (lat. 49.8189°N, long. 117.4549°W). A 2 m wide subvertical brittle dextral fault 172°/74° cuts across an east-dipping (008°/31°) ductile fabric of the Slocan Lake fault/Valkyr shear zone.

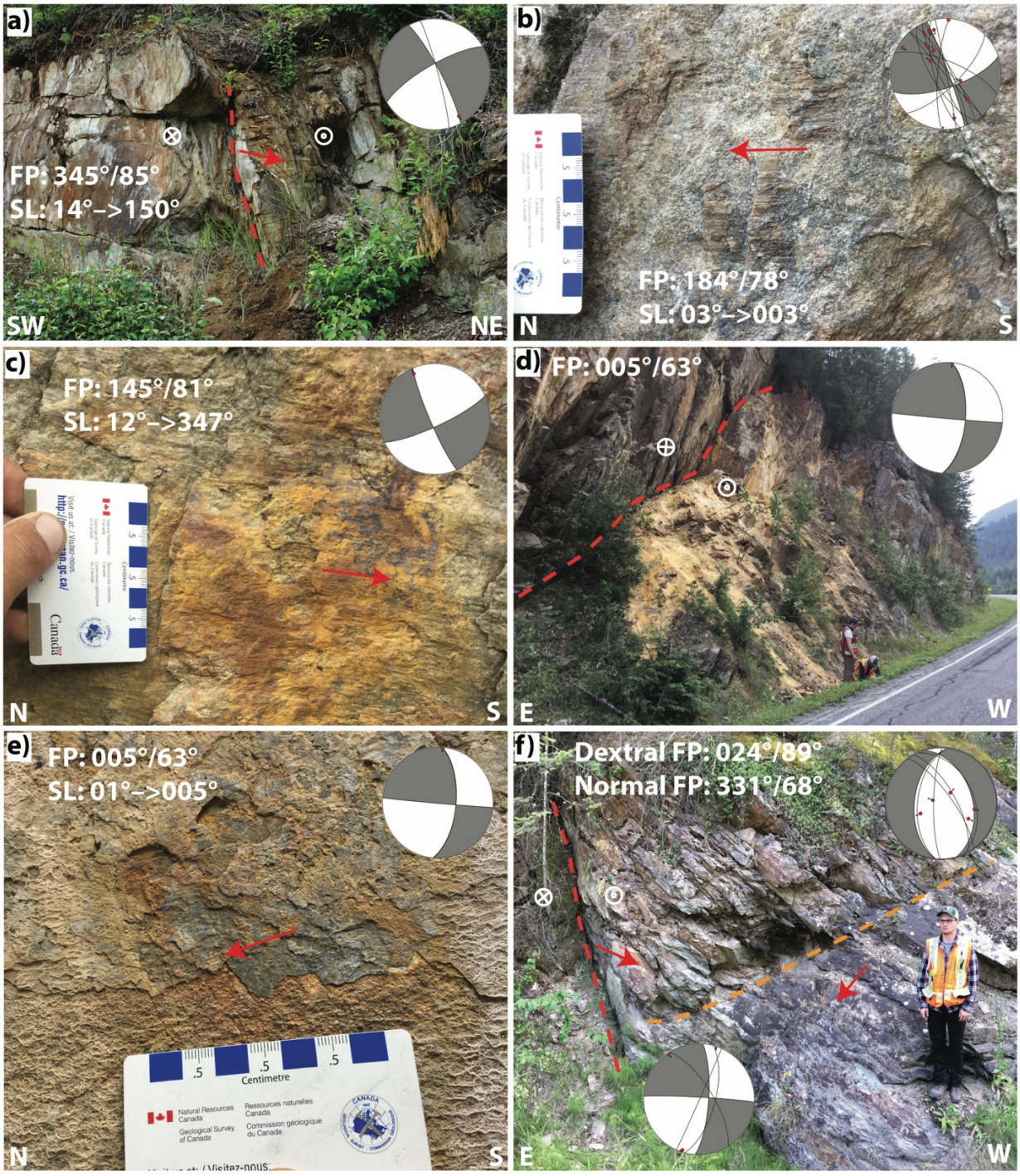
a)
FP: 345°/85°
SL: 14°–>150°
SW
NE
b)
FP: 184°/78°
SL: 03°–>003°
N
S
c)
FP: 145°/81°
SL: 12°–>347°
N
S
d)
FP: 005°/63°
E
W
e)
FP: 005°/63°
SL: 01°–>005°
N
S
f)
Dextral FP: 024°/89°
Normal FP: 331°/68°
E
W

1245

Figure 7. Photos from the Purcell Trench fault. See Figure 3 for photo locations. Beachballs show kinematics for each fault plane. Concentric circles indicate movement out of the page, circles containing an 'x' indicate movement into the page. a) Breccia and gouge zone at outcrop of the Adit fault near Beaton Arm (lat. 50.7025°N, long. 117.7095°W). Dextral slickenfibres (14°→150°) are present on a subvertical, limonitic fault plane (345°/85°). Rock hammer for scale. b) One of numerous dextral slickenfibres (03°→003°) observed on vertical fault zone (184°/78°) along Duncan Lake (lat. 50.4164°N, long. 116.9591°W). c) Dextral slickenfibres (12°→347°) on a limonitic subvertical fault plane (145°/81°) located 10 km north of Duncan Lake (lat. 50.6958°N, long. 117.1007°W). d) Dextral fault zone (005°/63°) on the western shore of Kootenay Lake near Kaslo (lat. 49.8524°N, long. 116.9032°W). e) Faint dextral slickenfibres (01°→005°) on the fault wall shown in e). f) A dextral fault (024°/89°) cross-cutting a normal fault (331°/68°) on the west side of the Purcell Trench along Highway 3 (lat. 49.1392°N, long. 116.6420°W).

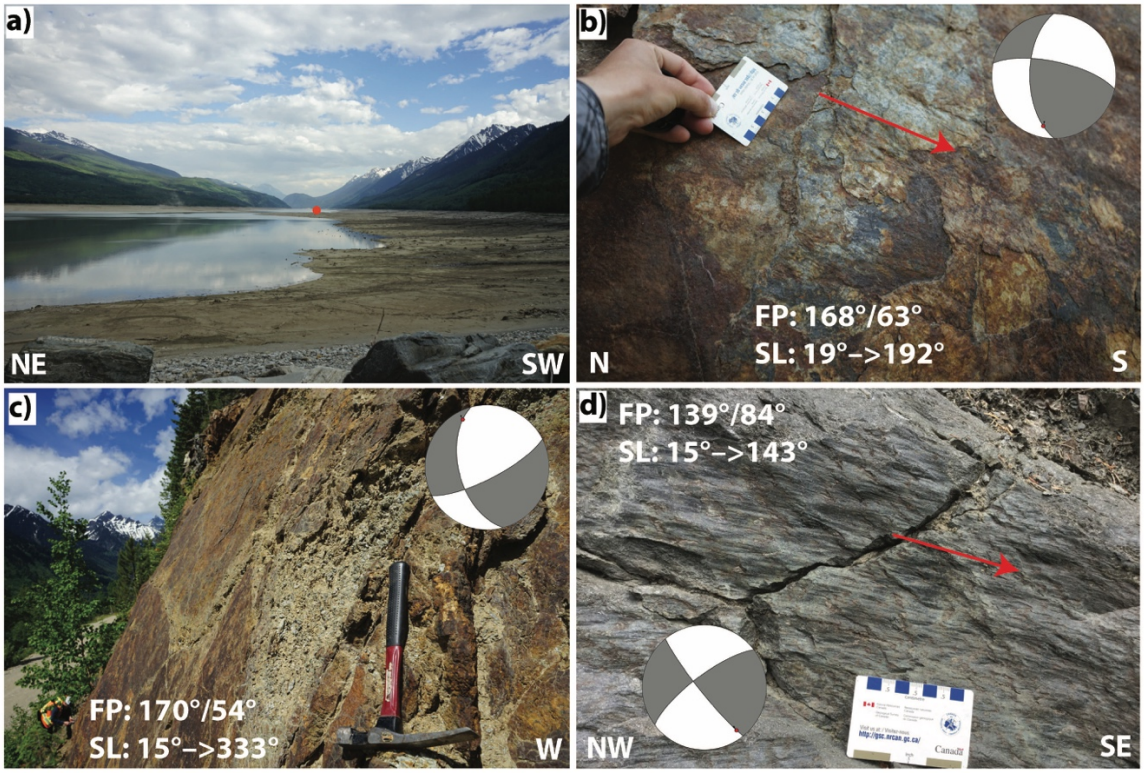

Figure 8. Photos from the Valemount/Canoe Reach area. See Figure 4 for photo locations and directions. Beachballs show kinematics for each fault plane. a) View south from the north end of the Kinbasket hydroelectric reservoir near Valemount, captured at low water level in May 2018. Red dot shows the location of the Canoe River thermal spring. b) Vestiges of dextral slickenfibres in basal Neoproterozoic Windermere Supergroup on the northeast side of the lake (lat. 52.5691°N, long. 118.8420°W). Fault is oriented 168°/63°, slickenfibres (red arrow) are oriented 19°→192°. c) Large, oxidized, fault plane in basal Windermere Supergroup on northeast side of lake (lat. 52.6202°N, long. 118.9424°W). Fault is oriented 170°/54°, dextral slickenfibres (not pictured) are oriented 15°→333°. d) Dextral slickenfibres in Paleoproterozoic Bulldog Gneiss on the northeast side of the lake (lat. 52.6412°N, long. 118.9759°W). Fault is oriented 139°/84°, slickenfibres (red arrow) are oriented 15°→143°.

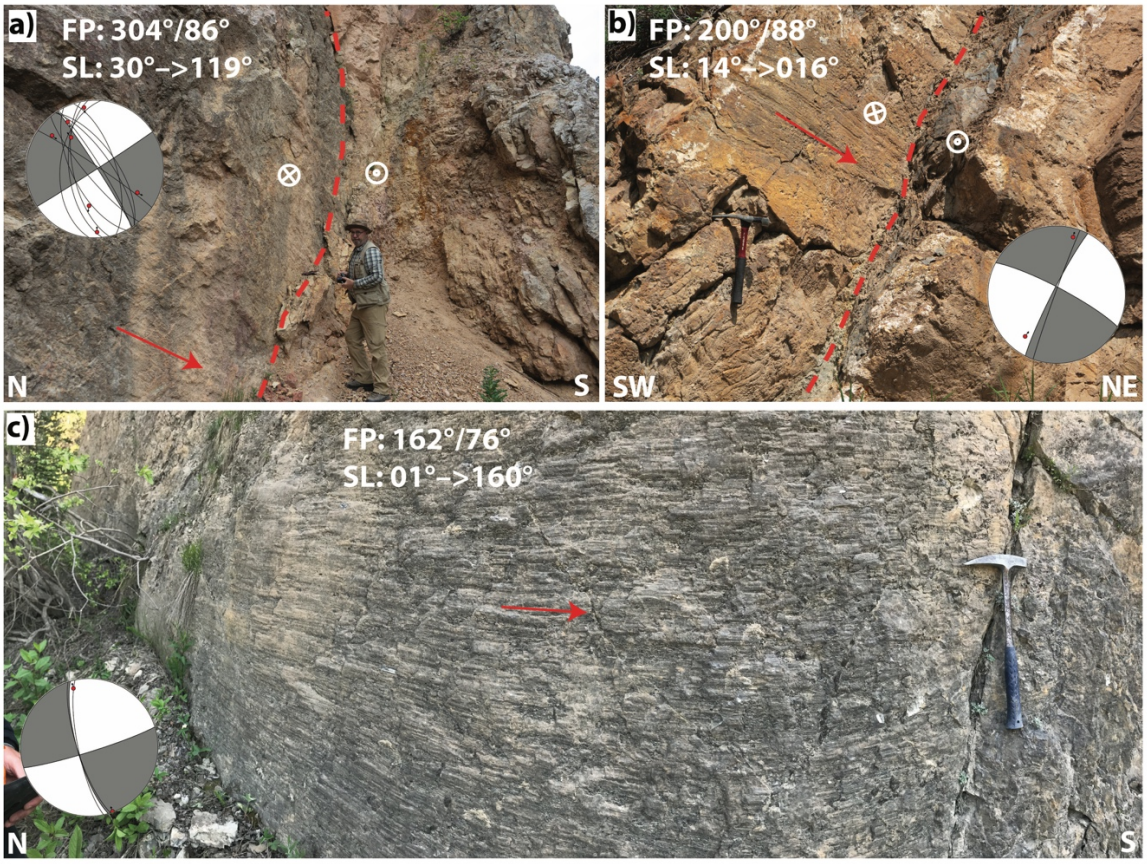

Figure 9. Photos from the Redwall fault and SRMT near Golden BC. See Figure 5 for photo locations. Beachballs show kinematics for each fault plane. Concentric circles indicate movement out of the page, circles containing an 'x' indicate movement into the page. a) Looking east at a dextral fault plane oriented 304°/86° within the Redwall fault zone near Radium Hot Springs (lat. 50.6356°N, long. 116.0372°W). Red arrow shows slickenfibre orientation (30°→119°). b) Oblique view from the southeast of dextral fault plane (200°/88°) with shallowly north-plunging corrugations (red arrow: 14°→016°) and shallowly south-plunging dextral slickenfibres (not visible: 25°→217°) near the south end of the Lussier River fault (lat. 49.7175°N, long. 115.5458°W). c) Looking east at a large fault plane (162°/76°) with abundant dextral slickenfibres (01°→160°) near the south end of Kinbasket Lake (51.6376°N, 117.4191°W).

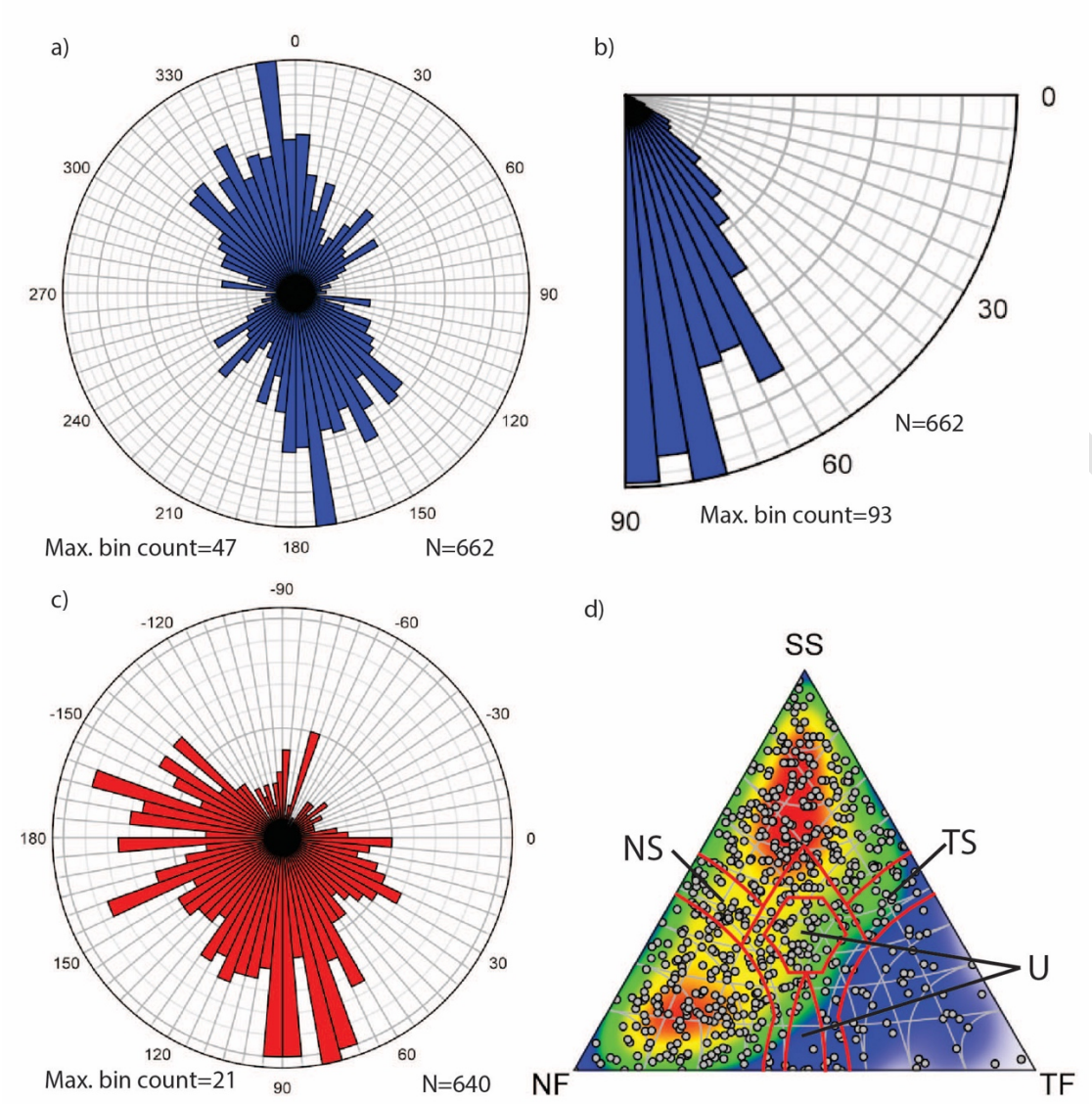

Figure 10. a) Bidirectional equal-distance circular histogram of the strikes of all 662 fault planes measured in this study. The strong NNW-SSE population is apparent, as is the subsidiary NE-SW population at high angles to the valleys. b) Unidirectional equal-distance quadrant histogram of the dips of all fault planes measured in this study. The majority are steeper than 60°. c) Unidirectional equal-distance circular histogram showing rake of slickenfibres on fault planes using the standard convention of hanging-wall motion relative to the foot-wall, such that 0° = sinistral, +90° = normal, 180° = dextral, and -90° = reverse. The largest populations are normal and dextral. d) Moment triangle (Frohlich, 1992) summarizing kinematic data based on the plunges of the calculated M, P, and T axes (Vollmer, 2019). Divisions of faulting styles are after Zoback (1992) and Balfour et al. (2011): SS = Strike Slip, NS = Normal Strike Slip, TS = Thrust Strike Slip, NF = Normal Faulting, TF = Thrust Faulting, U = undefined. Colour gradient illustrates the high concentrations (red) of strike-slip and normal faults.

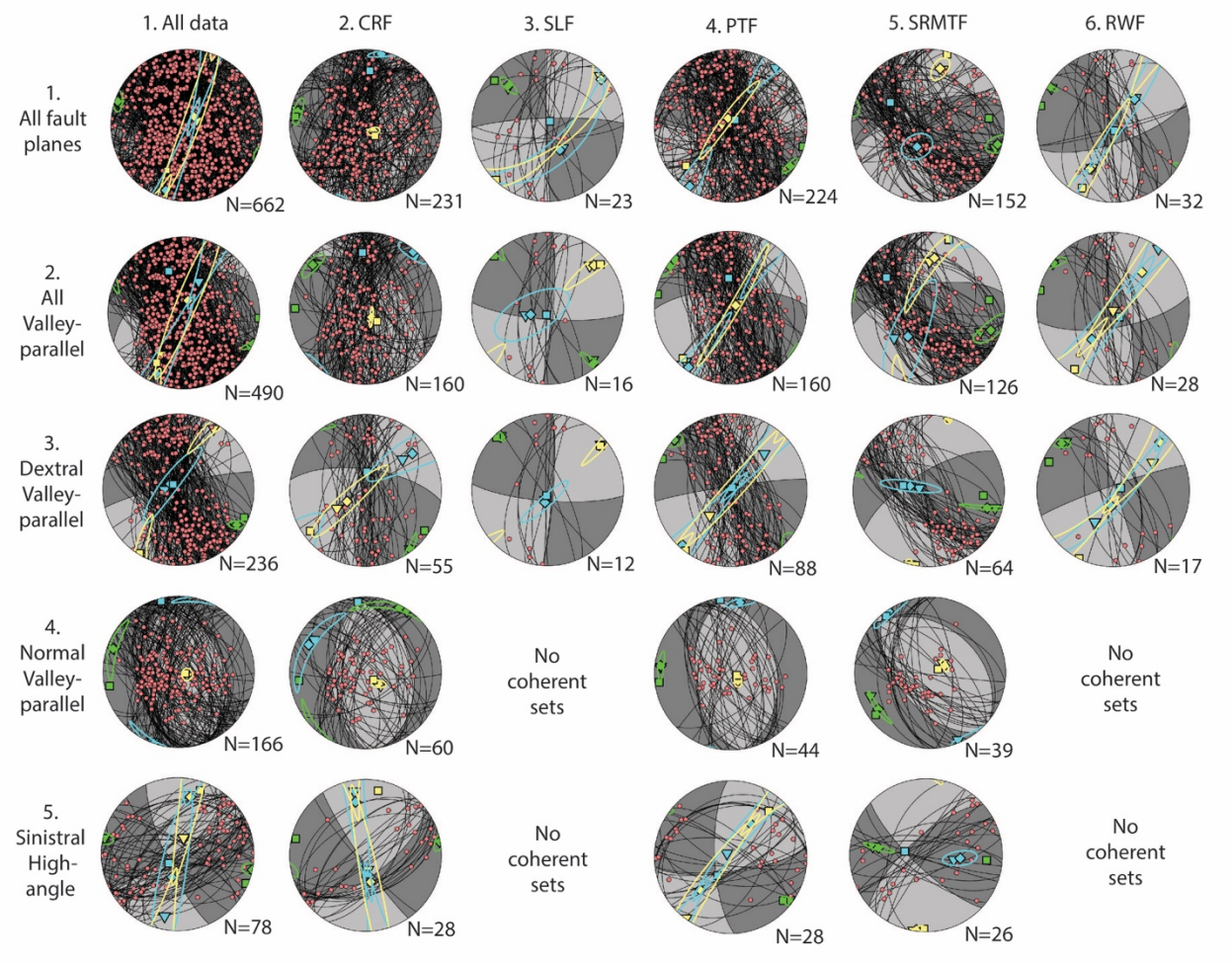

Figure 11. Equal area (Schmidt) lower-hemisphere beachball plots showing data from entire study area (column 1) and subdomains of each major fault zone (columns 2-6). Row 1 shows all unfiltered fault planes, row 2 shows all valley-parallel (<30° to the regional trend) fault planes, rows 3 and 4 show all valley-parallel dextral and normal faults respectively. Row 5 shows all sinistral faults oriented at high angles (>30°) to the valley, representing possible R' shears. Red dots are slickenlines, and black great circles are fault planes. Squares, triangles, and diamonds are respectively: average P-axes, best fitting principal stress axes, and average of the best 100 stress axis solutions. Yellow = P-axis and σ_1, blue = M and σ_2, green = T and σ_3. Confidence cones represent bootstrapped 95% confidence intervals for the best 100 principal stress axes for each domain, which illustrates the relative coherence of various subsets.

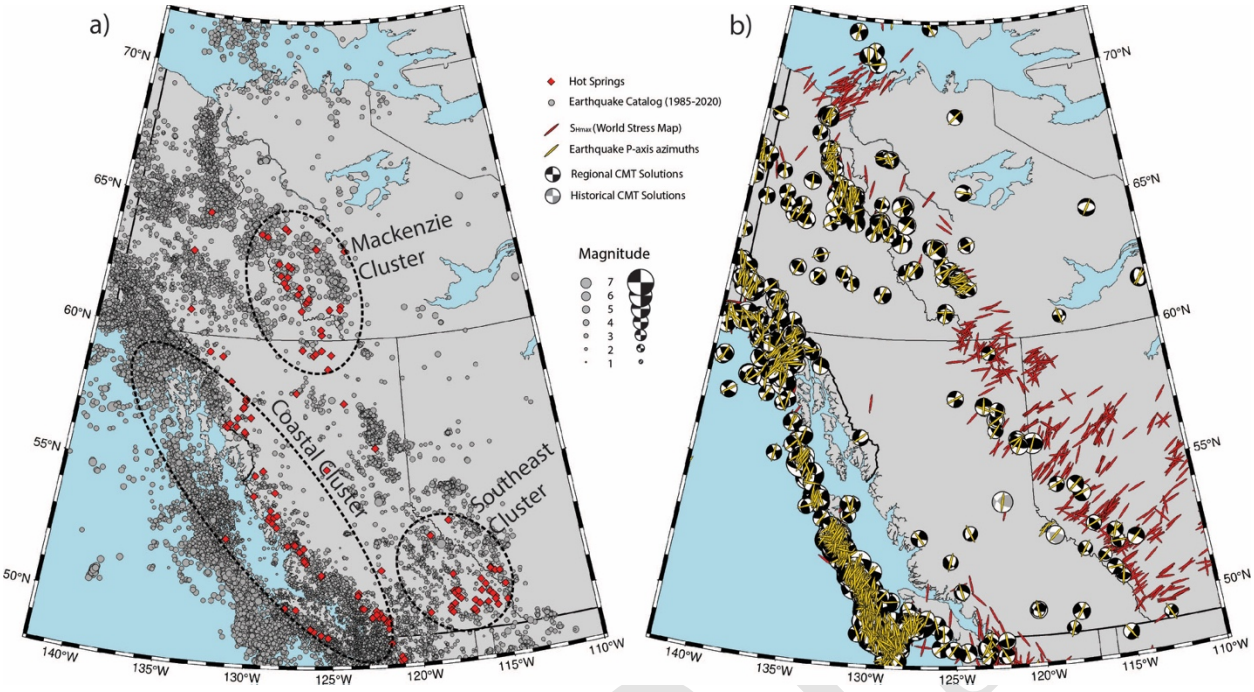

Figure 12. Relationships between seismicity, crustal stress, and thermal spring distribution. a) Thermal spring distribution compared to seismicity. Grey dots are all events in the Canadian National Earthquake Database from 1985 to 2020, scaled according to magnitude. Clusters of thermal springs are correlated with seismicity in three zones: the west coast, southern Mackenzie Mountains, and southeastern BC (this study). b) Stress and strain in western Canada. Beachballs represent the regional Centroid Moment Tensor (CMT) solutions for events > M 4 from 1985 to 2020 (Kao et al., 2012, Kao pers. comm. 2021) and focal mechanisms for the McNaughton Lake (1978) and Prince George (1986) earthquakes (Rogers et al., 1980, 1990) and two small events detected by Purba et al. (2021) near Valemount. Earthquake P-axes are shown as imperfect comparisons to S_{Hmax} orientations from the World Stress Map (Heidbach et al., 2018). This figure was plotted using GMT6 software (Wessel et al., 2019).

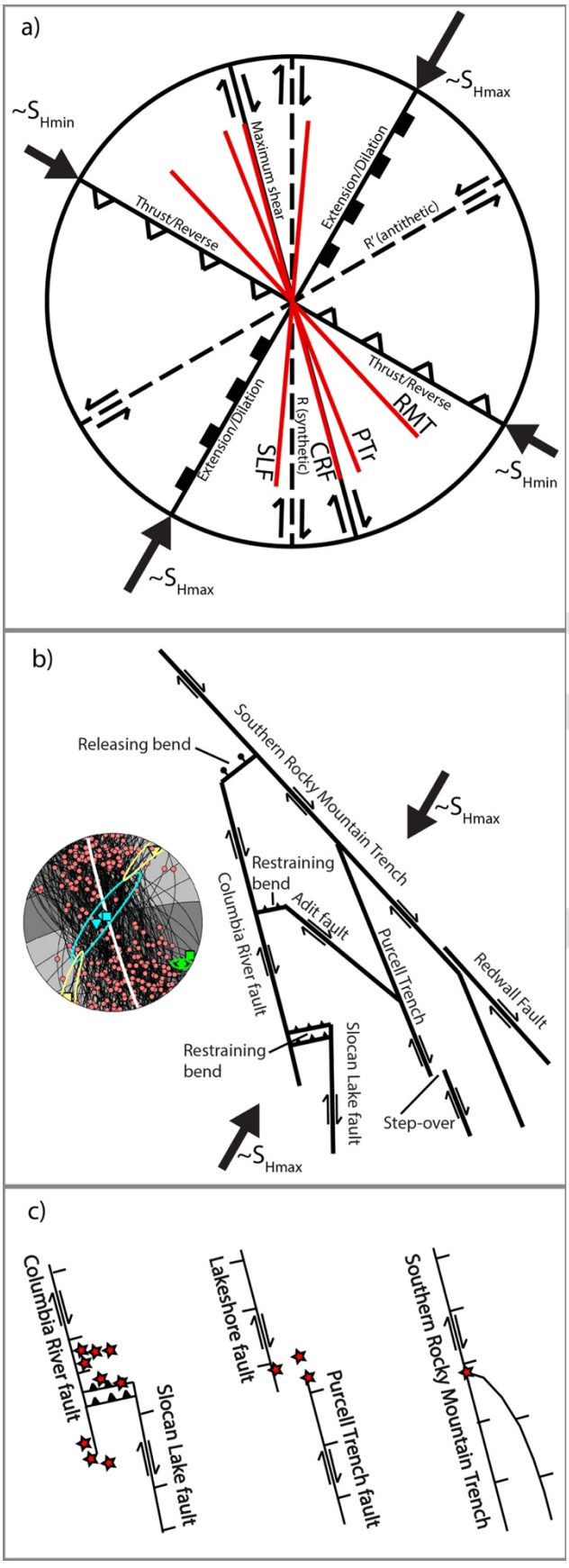
a)
~S Hmax
~S Hmin
Maximum shear
Extension/Dilation
R' (antithetic)
Thrust/Reverse
Thrust/Reverse
RMT
PTr
CRF
SLF
R (synthetic)
Extension/Dilation
~S Hmin
~S Hmax
b)
Releasing bend
Southern Rocky Mountain Trench
~S Hmax
Restraining bend
Adit fault
Columbia River fault
Purcell Trench
Redwall Fault
Restraining bend
Slocan Lake fault
Step-over
~S Hmax
c)
Columbia River fault
Slocan Lake fault
Lakeshore fault
Purcell Trench fault
Southern Rocky Mountain Trench

Figure 13. Relationships between current stress, fault kinematics and favourable structural settings. a) Strain ellipse for approximate S_{Hmax} orientation in southeastern BC (Ristau et al., 2007; Heidbach et al., 2018), and corresponding predicted modes of brittle deformation on faults and fractures. Average orientations of the SRMT fault, Purcell Trench fault, Columbia River fault, and Slocan Lake fault, are shown for reference. b) Schematic map of fault kinematics documented in this study. Stereoplot shows mean fault plane (white great circle), best fitting principal stress axes (triangles) and average P, M and T axes (squares) estimated for all dextral faults oriented parallel to the trend of the valleys (N=236). Yellow = P-axis and σ_1, blue = M and σ_2, green = T and σ_3 c) simplified structural settings favourable to specific thermal spring upwellings in southeastern BC.